Low-dimensional dynamics of large networks of spiking neurons

Synchrony-induced oscillatory dynamics

Jose M. Esnaola-Acebes

TESI DOCTORAL UPF / 2018

Thesis Supervisor:

Ernest Montbrió,
Department of Information and Communication Technologies

Escriviu aquí la vostra dedicatòria

Agraïments Agraeixo....

Resum

Vet aquí el resum de la tesi en català. Si us plau, utilitzeu menys de 150 paraules. Nam dui ligula, fringilla a, euismod sodales, sollicitudin vel, wisi. Morbi auctor lorem non justo. Nam lacus libero, pretium at, lobortis vitae, ultricies et, tellus. Donec aliquet, tortor sed accumsan bibendum, erat ligula aliquet magna, vitae ornare odio metus a mi. Morbi ac orci et nisl hendrerit mollis. Suspendisse ut massa. Cras nec ante. Pellentesque a nulla. Cum sociis natoque penatibus et magnis dis parturient montes, nascetur ridiculus mus. Aliquam tincidunt urna. Nulla ullamcorper vestibulum turpis. Pellentesque cursus luctus mauris.

Nulla malesuada porttitor diam. Donec felis erat, congue non, volutpat at, tincidunt tristique, libero. Vivamus viverra fermentum felis. Donec nonummy pellentesque ante. Phasellus adipiscing semper elit. Proin fermentum massa ac quam. Sed diam turpis, molestie vitae, placerat a, molestie nec, leo. Maecenas lacinia. Nam ipsum ligula, eleifend at, accumsan nec, suscipit a, ipsum. Morbi blandit ligula feugiat magna. Nunc eleifend consequat lorem. Sed lacinia nulla vitae enim. Pellentesque tincidunt purus vel magna. Integer non enim. Praesent euismod nunc eu purus. Donec bibendum quam in tellus. Nullam cursus pulvinar lectus. Donec et mi. Nam vulputate metus eu enim. Vestibulum pellentesque felis eu massa.

Quisque ullamcorper placerat ipsum. Cras nibh. Morbi vel justo vitae lacus tincidunt ultrices. Lorem ipsum dolor sit amet, consectetuer adipiscing elit. In hac habitasse platea dictumst. Integer tempus convallis augue. Etiam facilisis. Nunc elementum fermentum wisi. Aenean placerat. Ut imperdiet, enim sed gravida sollicitudin, felis odio placerat quam, ac pulvinar elit purus eget enim. Nunc vitae tortor. Proin tempus nibh sit amet nisl. Vivamus quis tortor vitae risus porta vehicula.

Laburpena

Laburpena euskaraz. Nam dui ligula, fringilla a, euismod sodales, sollicitudin vel, wisi. Morbi auctor lorem non justo. Nam lacus libero, pretium at, lobortis vitae, ultricies et, tellus. Donec aliquet, tortor sed accumsan bibendum, erat ligula aliquet magna, vitae ornare odio metus a mi. Morbi ac orci et nisl hendrerit mollis. Suspendisse ut massa. Cras nec ante. Pellentesque a nulla. Cum sociis natoque penatibus et magnis dis parturient montes, nascetur ridiculus mus. Aliquam tincidunt urna. Nulla ullamcorper vestibulum turpis. Pellentesque cursus luctus mauris.

Nulla malesuada porttitor diam. Donec felis erat, congue non, volutpat at, tincidunt tristique, libero. Vivamus viverra fermentum felis. Donec nonummy pellentesque ante. Phasellus adipiscing semper elit. Proin fermentum massa ac quam. Sed diam turpis, molestie vitae, placerat a, molestie nec, leo. Maecenas lacinia. Nam ipsum ligula, eleifend at, accumsan nec, suscipit a, ipsum. Morbi blandit ligula feugiat magna. Nunc eleifend consequat lorem. Sed lacinia nulla vitae enim. Pellentesque tincidunt purus vel magna. Integer non enim. Praesent euismod nunc eu purus. Donec bibendum quam in tellus. Nullam cursus pulvinar lectus. Donec et mi. Nam vulputate metus eu enim. Vestibulum pellentesque felis eu massa.

Quisque ullamcorper placerat ipsum. Cras nibh. Morbi vel justo vitae lacus tincidunt ultrices. Lorem ipsum dolor sit amet, consectetuer adipiscing elit. In hac habitasse platea dictumst. Integer tempus convallis augue. Etiam facilisis. Nunc elementum fermentum wisi. Aenean placerat. Ut imperdiet, enim sed gravida sollicitudin, felis odio placerat quam, ac pulvinar elit purus eget enim. Nunc vitae tortor. Proin tempus nibh sit amet nisl. Vivamus quis tortor vitae risus porta vehicula.

Resumen

Resumen en castellano. Nam dui ligula, fringilla a, euismod sodales, sollicitudin vel, wisi. Morbi auctor lorem non justo. Nam lacus libero, pretium at, lobortis vitae, ultricies et, tellus. Donec aliquet, tortor sed accumsan bibendum, erat ligula aliquet magna, vitae ornare odio metus a mi. Morbi ac orci et nisl hendrerit mollis. Suspendisse ut massa. Cras nec ante. Pellentesque a nulla. Cum sociis natoque penatibus et magnis dis parturient montes, nascetur ridiculus mus. Aliquam tincidunt urna. Nulla ullamcorper vestibulum turpis. Pellentesque cursus luctus mauris.

Nulla malesuada porttitor diam. Donec felis erat, congue non, volutpat at, tincidunt tristique, libero. Vivamus viverra fermentum felis. Donec nonummy pellentesque ante. Phasellus adipiscing semper elit. Proin fermentum massa ac quam. Sed diam turpis, molestie vitae, placerat a, molestie nec, leo. Maecenas lacinia. Nam ipsum ligula, eleifend at, accumsan nec, suscipit a, ipsum. Morbi blandit ligula feugiat magna. Nunc eleifend consequat lorem. Sed lacinia nulla vitae enim. Pellentesque tincidunt purus vel magna. Integer non enim. Praesent euismod nunc eu purus. Donec bibendum quam in tellus. Nullam cursus pulvinar lectus. Donec et mi. Nam vulputate metus eu enim. Vestibulum pellentesque felis eu massa.

Quisque ullamcorper placerat ipsum. Cras nibh. Morbi vel justo vitae lacus tincidunt ultrices. Lorem ipsum dolor sit amet, consectetuer adipiscing elit. In hac habitasse platea dictumst. Integer tempus convallis augue. Etiam facilisis. Nunc elementum fermentum wisi. Aenean placerat. Ut imperdiet, enim sed gravida sollicitudin, felis odio placerat quam, ac pulvinar elit purus eget enim. Nunc vitae tortor. Proin tempus nibh sit amet nisl. Vivamus quis tortor vitae risus porta vehicula.

Abstract

Oscillatory dynamics are one of the most observed features of neural activity. They are found across species in any region of the brain at almost any scale, from single neuron dynamics to whole brain activity. Typical recording techniques spanning large population of neurons show stereotypical oscillatory dynamics in many brain areas during a wide variety of cognitive tasks. As such, oscillations are thought to play an important role in information processing as part of both the encoding and the decoding processes. Studying the underlying mechanisms that originate such oscillations could help understanding *the overall brain functioning*.

Population models describing the average activity of large ensembles of neurons have been extensively used as a mathematical tool to investigate the fundamental laws responsible of such oscillations. However, classical population models fail in capturing synchronous activity in networks of neurons. In this thesis we explore this limitation by comparing their dynamics with simulations of spiking neurons. We focus our attention in analyzing the effect of collective synchronization in the macroscopic dynamics of neural populations and show that, synchronous activity plays an important role in generating transient and persistent oscillations in such networks, which are not capture by the traditional population models. In order to investigate the fundamental properties that originate such oscillations we use a novel firing rate model which is exactly derived from the population of spiking neurons where spike synchrony is also correctly described.

Keywords: mathematical neuroscience, oscillations, synchronization, neural population, firing rate, population model, spiking neurons, quadratic-integrate-and-fire, neural-field, mean-field.

Preface

Contents

Abstract ix

Preface xi

List of figures xvii

General Introduction 1

Chapter 1 OSCILLATORY DYNAMICS IN EXCITATORY-INHIBITORY NETWORKS OF SPIKING NEURONS 13

1.1. Case study: Simulations of spiking neural networks . . 19

1.2. Canonical firing rate (H-FR) and neural field models (H-NF) 20

1.3. Firing rate model of QIF neurons 22

1.3.1. Quadratic Integrate-and-Fire (QIF) model neuron 23

1.3.1.1. Theta neuron 26

1.3.2. Continuity equation for a population of QIF neurons . . . 26
1.3.2.1. Continuous formulation . . . 27
1.3.3. Dimensionality reduction: Lorentzian Ansatz . . 29
1.3.4. Solution to the continuity equation: QIF-FR equations . . . 33

Chapter 2 SYNCHRONY-INDUCED MODES OF OSCILLATION OF A NEURAL FIELD MODEL 35

2.1. Introduction . . . 37
2.2. Synchrony-induced modes of oscillation in Networks of QIF Neurons . . . 39
2.3. Neural Field model for quadratic integrate and fire neurons . . . 43
2.3.1. Effective QIF-NFM . . . 44
2.3.2. SHS and their stability: Synchrony-induced modes of oscillation . . . 45
2.3.3. Turing bifurcation and nonlinear stability of the SHS . . . 48
2.3.4. Synchrony-induced transient oscillations in bump states . . . 50
2.4. Conclusions . . . 52

Chapter Appendices . . . 55

2.A. Derivation of the QIF neural field model (QIF-NFM) . 55
2.A.1. Effective NFM model . . . 58
2.B. Linear stability analysis of the Spatially Homogeneous State . . . 58
2.B.1. Linear stability of the effective QIF-NFM Eq. (2.7) 58
2.B.2. Linear stability of the full QIF-NFM . . . 60
2.C. Small-amplitude equation near the Spatially Homogeneous State . . . 62
2.C.1. Critical eigenvectors . . . 62
2.C.2. Amplitude equation . . . 62
2.D. Numerical simulations . . . 67

2.D.1. Numerical simulation of the QIF model 67
2.D.2. Numerical simulation of the ring network 67

Chapter 3 SYNCHRONY-INDUCED PERSISTENT OSCILLATIONS IN A E-I NEURAL NETWORK 71

Conclusions 73

Appendix A GENERALIZATION OF THE QIF-FR MODEL 75

Appendix B NUMERICAL SIMULATIONS OF QIF NEURAL NETWORKS 77

References 91

List of Figures

1.1. Transient oscillations in LIF neural population. 16
1.2. Spatio-temporal patterns in networks of LIF spiking neurons. 20
1.3. Possible regimes of the QIF model neuron. 25
1.4. QIF membrane potential distribution and firing rate. . 31

2.1. E-I ring network schematics. 40
2.2. Transient synchrony in ring networks of QIF neurons . 42
2.3. Stability of SHS (J_K vs. $\bar{\eta}$). 46
2.4. Phase diagram of the QIF-NFM (J_K vs. $\bar{\eta}$). 49
2.5. Spectrum and FR profiles of BS. 51
2.D.1Euler integration of QIF neurons. 68

General Introduction

> *"Philosophy is written in this great book—by which I mean the universe—which stands always open to our view, but it cannot be understood unless one first learns how to comprehend the language and interpret the symbols in which it is written, and its symbols are triangles, circles, and other geometric figures, without which it is not humanly possible to comprehend even one word of it; without these one wanders in a dark labyrinth."*
>
> — Galileo Galilei, *Il Saggiatore* (The Assayer) (1623)

Since the pioneering discoveries of Santiago Ramon y Cajal and Camilo Golgi in the late 19th century which established the foundations of what we nowadays know as Neuroscience, extensive work has been done in order to understand the laws that shape neural dynamics. As in almost any natural science, the aim of scientists toward universal laws explaining our observations have push, from the very beginning, towards mathematical descriptions of the observed phenomena. With the birth of *neural theory* researchers sought to understand the secrets behind animal behavior looking into the microscopic constituents of its source: the neurons. Early in the 20th century, Louis Lapicque

introduced what is considered as the precursor of the famous integrate-and-fire model neuron (Brunel and Van Rossum, 2007b) (see also Brunel and Van Rossum, 2007a; Abbott, 1999), providing a first quantitative approach to the polarization process of neurons and the generation of the first spike after stimulus onset —what we know as the action potential. Theoretical neuroscience was born and following his work many phenomenological models describing the onset of the action potential were developed (Hill, 1936; McCulloch and Pitts, 1943; Stein, 1965; Geisler and Goldberg, 1966; Weiss, 1966; Stein, 1967).

In the 1950's Hodgkin and Huxley published the first detailed biophysical model of the action potential (Hodgkin and Huxley, 1952), a system of three differential equations which modeled the electrical currents across the cell membrane leading to action potentials in the squid's giant axon, and for which they received the Nobel price in 1963. Their almost 30 year investigation not only proved that detailed biophysical —yet simple and elegant— models of neural dynamics were possible, but also drove them to the hypothesis of the existence of ionic channels, which were confirmed only few decades later.

Modeling from the microscopic perspective: Spiking neuron models

Further development in the biophysical principles of neural dynamics was made with the study of additional cellular mechanisms involved in the reception and generation of the action potentials, such as different classes of ionic channels and pumps, synaptic transmission processes, etc. Currently, detailed biophysical modeling of single neurons remains a very active field of research where sophisticated models are continuously expanding our knowledge about neural mechanisms. On the other hand, the necessity of decreasing the complexity of neural systems lead many theoreticians towards simplified models of the neuron, where only the underlying mechanisms that generate the action potential were sought. We refer to these phenomenological models as point neurons or **spiking neuron** models. The first of its kind

was probably that developed by Lapicque which later evolved into the *leaky integrate-and-fire* (LIF) neuron model (Stein, 1965; Knight, 1972; Tuckwell, 1988).

The LIF model and the more general nonlinear integrate-and-fire models can be mathematically derived as limit cases of the Hodgkin-Huxley model (see for example Gerstner et al., 2014); they are typically presented in the form of an ordinary differential equation (ODE) describing the time evolution of the membrane potential $v(t)$ of the neuron, plus a resetting rule mimicking the generation of the action potential, which basically drives the potential back to a reset potential v_r after the neuron crosses a given threshold v_{th}. Their general mathematical form is (Abbott and Van Vreeswijk, 1993):

$$\tau_m \frac{dv}{dt} = f(v) + RI(t) \quad + \text{reseting rule involving } v_r \text{ and } v_{th}, \quad (1)$$

where $f(v)$ is the function that shapes the dynamics of the specific model (LIF, QIF, EIF, GIF, etc.), and $RI(t)$ corresponds to changes on the membrane potential due to input currents I (R denotes a constant input resistance). The time scale of the dynamics of the neuron are determined by the value of the membrane time constant τ_m.

As an exchange to reduce complexity, the precision with which the model reproduces electrophysiological measurements is sacrificed. However, due to the rather stereotyped shape of the action potential, it is unlikely that information transmission depends on its specific shape, but rather on its timing or frequency. Therefore, these models serve as an excellent tool to model spiking events and are much easier to analyze than complex biophysical or conductance models. In fact, since the outbreak of computer driven simulations, their elegance and simplicity has make them a widely used tool in the study of principles of neural information processing: the simplest LIF model is still the most popular of the *integrate-and-fire* family, but nonlinear models, such as the exponential-integrate-and-fire (EIF) (Fourcaud-Trocmé et al., 2003) and the quadratic-integrate-and-fire (QIF) (Ermentrout

and Kopell, 1986; Ermentrout, 1996) models are often considered as they better reproduce the spiking onset. The choice of the model rests upon the specific system we are willing to study, and what questions are we seeking to answer. For a thorough analysis on the dynamical properties of a great variety of spiking neuron models see Izhikevich (2007).

Yet, the outstanding number of neurons present in any small piece of cortex makes the brain one of the most complex systems ever studied. A universe inside our heads is still waiting to be discovered. Even if we considered the simplest phenomenological model neuron, and without taking into account any complex network structure, a simple model of the brain would consist on a system of approximately 86×10^9 differential equations –each describing the dynamics of a single neuron. A system impossible to work with, nor in the 20th century nor currently; even with the incredible computational power that we have at our hands. Any mathematical study involving so many differential equations is generally impossible to face, unless a proper reduction in dimensionality is done.

Practical matters aside, fundamental reasons concerning the statistical nature of neural populations (Cragg and Temperley, 1954), alongside other information theory-based hypothesis, suggested that collective, rather than single neuron dynamics, were more relevant in the information processing happening in the brain. With this paradigm in mind, models of population average activity started to appear, first in the 1950's by the hands of Beurle (1956), and later in the 1960's by Griffith (1963). They developed the first continuum approximations of neural activity by making some statistical assumptions, following a methodology closely related to that used in statistical physics in connection with thermodynamics. The aim was to create low dimensional models capable of capturing the essential collective properties of neural populations, yet simple enough to provide a mathematically tractable framework for their study.

In parallel, the rapid progress made in experimental neuroscience with studies such as those carried out by Mountcastle, and Hubel and

Wiesel in the somatosensory and visual cortex of cats and monkeys (Mountcastle, 1957; Hubel and Wiesel, 1962, 1968), gave support to the original hypothesis of Beurle. Moreover, in the early 1960's the first attempts to account for physiologically measurable phenomena in terms of the modeled properties of population of neurons were held by Freeman (1964). During the 1970's all these accumulation of experimental evidence inspired the work of many researchers, including Wilson and Cowan (1972, 1973), Knight (1972) and Amari (1972, 1974, 1977) among others, towards the development of population models, also known as *neural mass* models or *firing rate* models.

Looking to the whole picture from a low-dimensional perspective: Firing rate models

Population models were quickly accepted as valid descriptions of neural activity due to the increasing popularity of rate and population code* hypothesis—which assumes information is transmitted as the average activity of neurons and not by their individual spiking times (known as the time code hypothesis)—, plus the empirical evidence that pointed towards the existence of large redundancy among neural populations. Moreover, many brain measurement techniques, such as electroencephalography (EEG) and functional magnetic resonance imaging (fMRI), provide measures of averaged population activity taken as the average spike rate across populations distributed in relatively large areas of the cortex. All these, made firing-rate-based population models very useful tools not only as a theoretical construct but also as an experimental modeling tool (Destexhe and Sejnowski, 2009).

Among the various firing rate (FR) models developed in the 1970's,

*Although both, rate and population coding hypothesis, lie on the average activity of neurons, the former refers to the temporal average of spikes, while the latter refers to the population average. In an ergodic system, both hypothesis should be equivalent, however many neural systems show fast dynamics where the ergodic assumption is not likely to stand.

the Wilson and Cowan (WC) model is probably the most extended one due to its simplicity and versatility. It typically consists on an a set of two ODEs describing the time evolution of the activity of spatially lumped excitatory and inhibitory neural populations, measured as the fraction of active neurons in each population. Such activity is defined as the number of spikes per unit time, i.e. the firing rate. Space dependent firing rate models, also known as neural fields, are extensions of this model to continuously distributed populations of interacting excitatory and inhibitory neurons following some sort of network topology. In such cases, the model usually appears as a set of partial differential equations (PDE). In either case, models including temporal correlations, by adding synaptic kinetics, or axonal delays, require the use of integro-differential equations or additional differential equations modeling variables related to synaptic dynamics.

During the last 50 years, the WC model has been adapted or extended to account for different network configurations and to include a variety of physiologically relevant elements such as synaptic processes[cita] or axonal delays (Coombes et al., 2003; Roxin et al., 2005; Coombes and Laing, 2009; Roxin and Montbrió, 2011). Moreover, it is used not only to model population of neurons but also averaged activities of single neurons (measured as trial-to-trial averages) (e.g. Grossberg, 1973). However, these rate models are generally treated as 'ad hoc' models as they are not derived from the dynamics of the microscopic elements that constitute the studied system: the neurons. In other words, the derivation of rate equations does not follow a proper reduction of the microscopic neural system. Moreover, traditional firing rate models assume microstates where neurons' activity is fully or highly uncorrelated. in order to simplify their mathematical expressions. Therefore they usually fail to describe any dynamical phenomena occurring as a consequence of synchronous firing. These phenomena may include fast transients and some types of persistent oscillations observed in their homologous spiking neural networks.

One of the goals of this work is to understand the effect that synchronized states (transient or persistent) have in the macroscopic

dynamics. Therefore, we find convenient to summarize the main assumptions and simplifications usually followed in the derivation of traditional firing rate models. A quick revision to the seminal work of Wilson and Cowan (1972) reveals some of the typical assumptions made for obtaining this type of firing rate equations:

i) The heterogeneity of neural population, modeled as the distribution of a given microscopic neural parameter, is generally averaged out to a single macroscopic variable. In their paper, the mean field approach reduces the apparent distribution of neurons, taken as a distribution on the number of afferent synapses per cell, to the neural response function $\mathcal{S}$. This assumption states that all neurons are behaving equally following a relevant observable that only describes the average value of the distribution of neurons. And therefore, ignores any dynamical effects that higher moments of the distribution may have over the macroscopic dynamics.

ii) Correlations between the level of excitation of a cell and the probability that the cell is sensitive are assumed to be negligible. This assumption is neglecting any effects related to the heterogeneous distribution of neurons, i.e. any dynamical regime which rests upon the specific time evolution of the distribution of the states of the neurons will be lost. This, along with the previous reduction, further decreases the effect of microscopic diversity in the macroscopic behavior. E.g.: in an heterogeneous population of neurons, some of the neurons may be in the refractory period while others are close to threshold; the effect that the response function has over them will vary, and therefore it will create correlations. These correlations will further depend on the specific dynamics of the membrane potentials of neurons.

iii) Probably, the most famous simplification is that of the *time coarse graining*: by considering that synaptic activation behaves as a low-pass filter, the authors reduce the temporal integrals to time-averaged quantities, thus reducing the original system composed

of a couple of integro-differential equations to that of a couple of ODEs, much easier to treat analytically. This simplification prevents any fast transient dynamics occurring as a consequence of synaptic kinetics, such as some type of damped oscillations. In general, this situation is easy to overcome by the inclusion of at least* an additional equation for the dynamics of the synapses. However, the system becomes 4-dimensional and consequently much harder to mathematically analyze.

We are mainly interested on the simplifications done to reduce the intrinsic dimensionality given by the neural diversity, i.e., those statistical assumptions related to the distribution of membrane potentials. Summarizing the above assumptions, the WC firing rate model heuristically sets the firing rate of the population to the firing rate of the *typical* neuron in the network, that is, the one with the mean parameters. This explains why the model is also used to describe the firing rate of single neurons under stochastic fluctuations.

The bridge between the micro and the macro

Since the emergence of the first population models, many studies have address all these issues from different perspectives. The so called *integral-equation* approach —in which we may include the original WC 1972 model— defines the state of the system by means of a probability density function $P_I\left(t|\hat{t}_i\right)$ describing the probability that the next spike occurs around time t given that the last spike was at time $\tilde{t}_i$ and the neuron was subject to an input $I\left(t'\right)$, $t < t'$ (Gerstner et al., 2014). Thus, neuronal activity is interpreted in terms of the interspike interval (ISI) distribution. This methodology, which can be extended to account for neural adaptation (Naud and Gerstner, 2012), and heterogeneous populations (modeled as noisy neurons (Gerstner, 2000)), successfully captures many of the fast dynamics caused by

*A general model of synaptic kinetics is the alpha function, which accounts for both rise and decay of synaptic activation described by a second order ODE, with different time constants for each process.

heterogeneity and also synaptic kinetics. However, it is generally difficult to write down an exact analytical formula for the probability density P_I, and the subsequent mathematical analysis is not an easy task. Moreover, the use of such models involves complex numerical methods which makes them unpopular among experimental researchers in contrast to the much simpler WC firing rate equations.

On the other hand, methods focusing on the *population density* were inspired by previous works in statistical physics. Amari (1972) faced the problem of population dynamics in a way closely related to the approach followed by Knight (1972); the idea is to apply the thermodynamic limit and define a membrane potential density equation for the population of neurons. Next, due to the conservation of neurons, the continuity equation can be applied. Theoretically, macroscopic observables, such as the firing rate or the mean membrane potential of the population should be related to the macroscopic quantities that determine the distribution of membrane potentials. Furthermore, knowledge of the momentary distribution of membrane potentials should be enough to characterize the momentary state of the population as a whole.

The main challenge here, as it also happens for the integral-equation approach, is to determine the distribution of membrane potential and its temporal evolution. To be able to tackle this situation, statistical assumptions related to neuronal populations are applied, often inspired by simulations of their constituent spiking neurons, or focusing on particular dynamical states. Typical examples assume uniform or normal distributions for membrane potentials, uncorrelated populations, diffusion driven dynamics. etc. Usually, such simplifications lead to well known mathematical descriptions like the Fokker-Plank (FP) equation (Risken, 1989; Abbott and Van Vreeswijk, 1993; Brunel and Hakim, 1999; Brunel, 2000; Knight et al., 2000; Nykamp and Tranchina, 2000; Brunel et al., 2001; Fourcaud and Brunel, 2002). In any case, the population density approach is closely related to that of the integral-equation, and a formal mathematical relation between both approaches exists for certain neuron models (Gerstner et al.,

2014).

As it happens with the integral equation, not only is difficult to asses the impact that simplifications have in the macroscopic dynamics of the population, but also they often lead to complex mathematical formulations which require numerical methods for their application as population models (for a robust numerical integration of the FP equation for integrate-and-fire type neural populations see Richardson (2007, 2009)). Yet, the development of all these models has greatly contributed to the understanding of the underlying mechanisms of the macroscopic dynamics of networks of spiking neurons (Fusi and Mattia, 1999; Omurtag et al., 2000).

Finally, a third family of population models is worth mentioning. The so-called *neural mass* models (also known simply as neural population models) refer to a class of models that describe the temporal evolution of one or more statistical moments that characterize the dynamical state of the neural system (Liley, 2013). They are generally focused on describing the temporal evolution of the mean membrane potential rather than the firing rate, although they commonly include a mathematical expression that binds both macroscopic quantities. Such models are closely related to the approach followed by Amari (1972) in the fact that they consider not only mean quantities related to the population distribution, but also second order or higher moments relevant to the macroscopic dynamics of the population. Highly influenced by the work of Lopes da Silva et al. (1974), typical neural-mass models follow the reasoning approach of Freeman (1975), and their current canonical form is the Jansen-Rit model (Jansen et al., 1993; Jansen and Rit, 1995). This latter model contains three interconnected neural populations with a set of feedback loops, where each population is described by as second-order (linear) differential operator transforming the incoming mean firing rate to the mean potential. In addition, a nonlinear function transforms the mean membrane potential back to a mean output firing rate quantity (Knösche, 2014).

Their main advantage is the ability to produce a wide variety of dynamical regimes by means of a rather simple low-dimensional model.

This feature makes it particularly efficient in modeling large-scale activity of the brain (Deco et al., 2008). However, its phenomenological construction makes difficult to dig into the most subtle mechanisms involving the subthreshold dynamics of neural populations.

Objectives

In light of the limitations of traditional FR models to explain some of the collective behaviors observed in spiking neural networks, in this work we exploit a recently published FR model (Montbrió et al., 2015) to understand the mechanisms behind some of the fast macroscopic dynamics observed in populations of spiking neurons. This novel FR model (see section 1.3) is exactly derived from a network of quadratic-integrate-and-fire (QIF) neurons and therefore provides an exact link between the spiking neuron simulations and the FR equations. We will refer to this model as the **QIF-FR** model in contrast to the traditional and heuristically derived WC firing rate model, which we name as **H-FR** model. The QIF-FR model consists on a system of coupled ODEs susceptible to an analytical study, and it will provide us with valuable information to better understand the microscopic mechanisms behind the observed macroscopic dynamics.

In Chapter I we start by reviewing the common mechanisms describing the onset of oscillatory activity in excitatory-inhibitory neuronal ensembles, and we perform some numerical experiments were we compare results obtained from simulations of spiking neural networks with their equivalent mean-field representation, modeled using the H-FR equations (H-FREs). Next by performing linear stability analysis on the H-FREs we demonstrate that some observed oscillatory dynamics can not be capture by them, which motivates us to use the QIF-FREs. In the following chapters, we systematically apply this model as a tool to study the dynamics of networks of excitatory and inhibitory neurons.

In Chapter II we extend the QIF-FR model into a neural field model (QIF-NF) to study the dynamics of a ring network of excitatory

and inhibitory neurons with non-local all-to-all coupling. Here we focus on the network's response to spatially modulated perturbations and define what we call the *modes of oscillation* of a neural network. We discuss about the relation between such macroscopic modes and their relation to transient synchronization of the neural population.

Further research of oscillatory dynamics in networks of excitatory and inhibitory neurons requires the incorporation of synaptic dynamics into the model, and also the necessity of explicitly differentiate excitatory and inhibitory populations (by changing the intrinsic properties of the neural populations). As a first step, in Chapter III we analyze the spatially flat state (spatially homogeneous state) using an equivalent two population firing rate description, i.e. a typical E-I neural setup (Wilson and Cowan, 1972). Following the same methodology as in Chapter II, we seek to understand the mechanisms that give rise to oscillatory behaviors. In order to proof the role of population synchronization in the generation of persistent oscillations we compare our QIF neural network to an equivalent system of Kuramoto oscillators allowing us to qualitatively compare the macroscopic dynamics of both systems. We find that some type of oscillations are consequence of a complex *two stage* synchronization-resonance process.

Finally, we summarize and discuss the role of synchronous activity in the generation of collective oscillations, which are not captured by traditional firing rate models. We also comment on the most relevant features and limitations of the QIF-FR model, and the plausibility of such systems in actual neural networks.

CHAPTER 1

Oscillatory dynamics in excitatory-inhibitory networks of spiking neurons

"There cannot be a language more universal and more simple, more free from errors and from obscurities, that is to say more worthy to express the invariable relations of natural things"

— Joseph Fourier, The Analytical Theory of Heat (1878)

This general introductory Chapter aims to motivate the questions that inspired this thesis (sections 1.1 and 1.2), and also serves as the presentation of the model that allowed us to quantitatively address such questions (section 1.3).

Here we ask the following questions: what minimal conditions must be fulfilled in order to construct a neural mechanism capable of generating macroscopic oscillatory activity? what is the role of neural diversity in shaping such phenomena? are traditional firing rate models capable of capturing these collective dynamics?

We start by reviewing possible mechanisms described in the literature which ought to explain rhythmogenesis in local populations

of excitatory (E) and inhibitory (I) neurons. By focusing on either fast transients or persistent activity, we formulate an early hypothesis about the origin of some of the rhythms we observe in spiking neural networks. To test the validity of such hypothesis we perform simulations of spiking neurons which satisfy the minimal conditions needed to observe oscillatory behaviors. Afterwards, we test the capability of H-FR models to reproduce such behaviors. We finish the chapter by introducing the QIF-FR model, which will be used as our preferred modeling tool through the rest of the work.

Rhythmogenesis in neural populations: transient and persistent oscillatory dynamics

Almost a century has passed since the rather esoteric discovery of the electroencephalogram (EEG) and the alpha waves by Berger (1929) and other contemporary researchers. Since then, oscillatory dynamics has been reported and categorized according to their frequency, location in the brain, relation to particular conscious states, etc (Buzsaki, 2004). As a consequence, we now have a cacophony of oscillatory behaviors which are categorized according to their observation circumstances. This universal presence of oscillations in the activity of the brain strongly suggests their relation to numerous brain functions (Buzsaki, 2004; Buzsáki and Moser, 2013). However, the discussion on the functionality of oscillations is out of the scope of this work *, in contrast, our interest is more devoted to dig into the mechanisms involved in their arousal.

We will limit our work to particular cases involving localized populations of excitatory (E) and inhibitory (I) neurons. Note however, that in Chapter 2 we derive a neural field model with nonlocal connectivity. Despite the model exhibiting *angular* dependence (in addition to temporal dependence), it is not a model accounting for the typical spatial activity propagation, but rather a mean field model where

*For a broad introduction about brain rhythms, with an approach that goes beyond mathematical and philological aspects of the matter, see Buzsaki (2006).

neurons are characterized for having selectivity to spatially modulated inputs. As such, the mathematical description is not given in the form of PDE, but in the form of integro-differential equations. This approach normally intends to describe dynamics occurring at small regions of the cortex or the hippocampus, where a certain homogeneity in neurons properties can be assumed. All these constrains normally imply the appearance of fast oscillations, in contrast with the slow dynamics typically measured in studies involving whole brain activity, such as resting state dynamics. In our path towards the study of the role of collective synchronization in oscillatory dynamics, we first investigate fast transient responses, and afterwards, expand our research to persistent oscillations. We would first like to add a word of caution about what we understand as *mechanisms* and *concepts* underlying specific dynamics in neuronal populations. We understand concepts as substrate independent, whereas mechanisms depend on given substrates which could respond to more general concepts. For example, oscillations are generally generated as an interplay between negative and positive feedback processes, but their manifestation in neural populations can be produced by different mechanisms.

Transient episodes of oscillatory dynamics

We define transient oscillations as relatively fast (of the order of the membrane time constant of neurons) episodes of oscillatory dynamics which arise as a consequence of an external perturbation (e.g. a momentary step current applied directly to the neurons) and which fade out after a certain duration after the perturbation, normally in the form of damped oscillations and in a way similar to the damped harmonic oscillator. An example of such oscillations is shown in Fig. 1.1. Physiological studies reporting similar dynamics go back to the 1960s where damped oscillations were observed in evoked potential studies (Freeman, 1967, 1968a,b; Andersen and Eccles, 1962) and more recently, in studies performed *in vitro* preparations (Silberberg et al., 2004; Tchumatchenko et al., 2011).

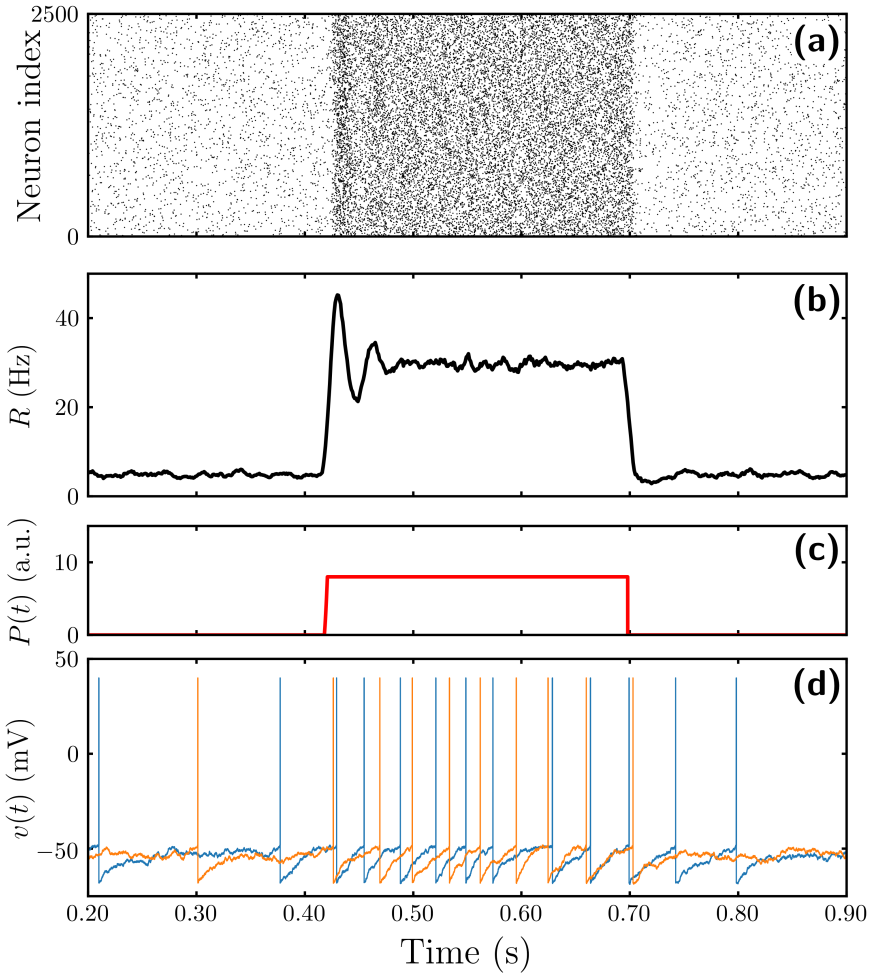

Figure 1.1: Fast transient response of a population of noisy LIF model neurons [Eq. (1)] to an abruptly injected step current $P(t)$. Panel (a) and (b) show, respectively, the raster and the instantaneous firing rate activity $R(t)$ of a population of $N = 2500$ LIF neurons subject to uncorrelated random inputs modeled as GWN of mean $\bar{\eta} = -2$ mV and width $\sigma = 5.0$ mV. At 0.4 s a step current of duration 0.3 s is applied as shown in panel (c). In panel (d) the membrane potential $v(t)$ of two randomly chosen neurons are shown. Parameters characterizing individual LIF neurons are $v_{th} = -48$ mV, $v_r = -68$ mV, $E = -50$ mV, $\tau_m = 20$ ms. See Appendix[cita] for details of the numerical simulations.

The theoretical aspects of transient responses were already studied by Knight (1972) and Wilson and Cowan (1972), who tackle the observed phenomena from fundamentally different perspectives. Although the resulting oscillatory dynamics were qualitatively similar, and their time scales could be adjusted so that their frequency matched, the underlying mechanisms generating such oscillations were different. A difference which is further reflected by the methodology they used.

On one hand, fast transients in the population activity of spiking neurons can be attributable to their intrinsic dynamics, and arise independently of the specific synaptic dynamics. As such, the population activity responds to big and rapid changes in the input currents in a relatively fast manner, characterized by the membrane time constant, in contrast to the slow temporal scales related to synaptic kinetics. This observations have been reported in studies dealing with spiking neuron networks and supported by experimental data obtained *in vitro* preparations (see e.g Gerstner, 2000; Brunel et al., 2001; Silberberg et al., 2004; Naud and Gerstner, 2012). In the following we show that oscillatory transients can be observed in networks of spiking neurons without synaptic couplings, which suggest the existence of a collective mechanism generating such dynamics.

On the other hand, Wilson and Cowan modeled similar dynamics using the integral-equation approach, i.e. the WC model prior to the time-coarse graining simplification. It is generally hard to draw conclusions based on traditional firing rate equations due to their blurry relationship with the microscopic state they represent, nevertheless it is straightforward to see that the reported oscillations in WC integral-equation model are entirely attributable to synaptic dynamics represented in the temporal integral. An observation which they emphasized in the derivation of the simplified version of the model and which we show later. These oscillations therefore, reflect a a potentially alternative mechanism of ryhtmogenesis, based on the synaptic time delays rather than on the intrinsic dynamics of neurons. This feature is explicitly included in more general integral-equations, and also in recent extensions of the WC model describing synaptic

kinetics (modeled as additional ODEs).

Persistent oscillatory dynamics

The link between transient and persistent dynamics is not trivial, and extrapolating the above hypothesis to infer possible mechanisms behind the generation of persistent oscillation is not straightforward. Even less when we consider the joint effect of synaptic kinetics and collective synchronization. Thus, following our aim of understanding the role of collective synchronization in the generation of oscillatory dynamics, we will consider the simplest possible scenario in which persistent oscillations arise.

Generally speaking, oscillations occur as the interplay between fast excitatory versus slow inhibitory feedback processes for which neural systems offer a variety of compatible mechanisms. Following systematic studies in the generation and modulation of gamma rhythms in hippocampal slices (Gloveli et al., 2010; Whittington et al., 2011), fast oscillations are categorized into three groups. Namely, Interneuron Network Gamma (ING), Pyramidal Interneuron Network Gamma (PING) and Persistent Gamma (PG). The first type are associated to oscillations occurring due to purely inhibitory activity whereas PING oscillations require the interplay between excitatory neurons (also known as principal neurons) and inhibitory interneurons. The last category is given to oscillations involving also both types of cells, but where excitatory neurons fire at low rates as compared to those observed during PING oscillations. In addition, PG oscillations persist considerately longer that ING or PING. Still, this categorization mainly accounts for the physiological circumstances in which these oscillations are observed (generally *in vitro*), and to some extent on the qualitative observations of both the macroscopic dynamics and the response of individual neurons. In fact, all three descriptions admit more than one compatible mechanism, and they are not mutually exclusive. In any case, *in vivo* activity is more likely to be composed of a mixture of the three rhythms where synchronization is commonly

assume to play a decisive role.

Extensive theoretical research exists around the principles of ING generation (Whittington et al., 1995; Wang and Buzsáki, 1996; White et al., 1998; Tiesinga and Jose, 2000; Whittington et al., 2000; Brunel and Hansel, 2006; Bartos et al., 2007; Wang, 2010), however we are interested in populations where excitatory neurons play a significant role in shaping macroscopic dynamics. Therefore, we will not discuss ING oscillations in this thesis, but many conclusions obtained in this work are also applicable to those type of networks and have been discussed by e.g. Devalle et al. (2017).

1.1 Case study: Simulations of spiking neural networks

In the following examples we present two different configurations of such networks. The first one will consist on a typical orientation selectivity neural field, where neurons are spatially arranged in a ring network. In the second example we investigate a two population excitatory-inhibitory network, with recurrent and cross coupling connectivity.

We start by considering a network of spiking neurons in a steady homogeneous state, also known as the asynchronous state

- Hodgkin-Huxley, and IF models.
- Conductance-based and current-based IF models.
- Type I and type II. Transfer function.
- Comparison of different spiking neuron models: their viability and biological plausibility. *Intro?*

Observation I: decaying oscillations in a spatially E-I distributed network

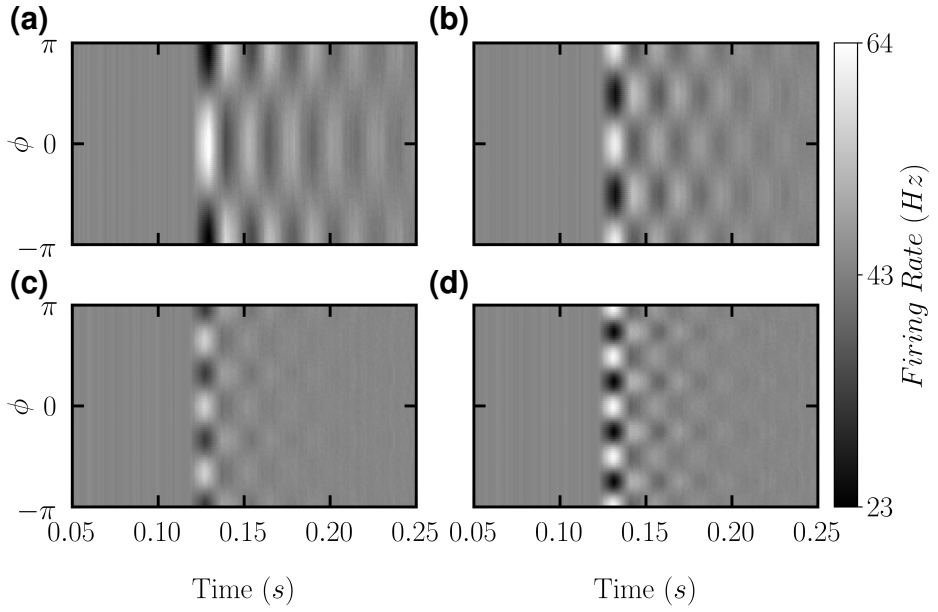

Figure 1.2: Transient episodes of spike synchrony in heterogeneous ring networks of $N = 2 \cdot 10^5$ LIF neurons, $J_0^e = 6.0$, $J_1^e = 2.5$, $J_2^e = 1.875$, $J_3^e = -0.75$, $J_0^i = -6$.

Observation II: persistent oscillations in a two population E-I model

1.2 Canonical firing rate (H-FR) and neural field models (H-NF)

Previously shown simulations consist on populations of spiking neurons of the order of $N = 10^5$, and they present incredibly rich dynamics when even for small number of parameters. Being such extensive sys-

tems they pose huge difficulties when trying to study them numerically. To be able to cope with this situation researchers in computational neuroscience have been developing mean field approximations which describe the population dynamics using some kind of macroscopic observable. Among others the most used measure is the firing rate of the population, which is a measurable magnitude using standard techniques of electrophysiology. The firing rate is the number of spikes emitted by the population in a given time interval.

Models of firing rate estimate the probability of spike of the individual neurons and average over time giving a measure of the instantaneous activity of the network. They typically have the form of integro-differential functions which can be feasibly simulated and often allow a variety of analytical study.

Among the numerous FR models used in computational neuroscience there is a family known as the Wilson-Cowan (WC) FR models from the seminal work of the authors with its name in 1972 and 1973. WC model consists on a one dimensional differential equation

- Macroscopic magnitudes involving the activity of neurons.
- Firing rate models: Wilson-Cowan type FR models. Heuristically obtained. Asynchronous activity of neurons as a fundamental assumption. They are not able to capture the transient dynamics of neural populations. (Neurons assumed to be completely uncorrelated).
- Probabilistic approaches: Fokker-Planck equation. (Diffusion limit).
- Spatially extended models: description of population of neurons in a continuum space. Cortical layers, orientation selectivity, whole brain modeling: waves.
- They provide a framework to be able to compare theoretical results with experimental findings. Guide new experimental studies based on theoretical findings.

- We present a new firing rate model that is exactly derived from the dynamics of single neurons, and therefore is able to describe novel collective dynamics due to the correlations between neurons, such as synchronization, partial synchronization, transient synchronization. We show that these collective dynamics

1.3 Firing rate model of QIF neurons (QIF-FR)

As was shown in the preceding section, canonical FR models fail to describe population dynamics in which a significant fraction of the neurons fire synchronously. In the simulations of section 1.1 we could observe that synchronous firing occur not only due to external drive (Case I 1.1) but also to some degree during spontaneously generated network states (Case II 1.1).

In this section we present a recently published set of exact macroscopic equations for quadratic integrate-and-fire neurons (QIF-FRE) which explicitly take into account subthreshold integration (Montbrió et al., 2015). In subsequent chapters we will be using these set of equations along with their equivalent microscopic representation, i.e. simulations of QIF neurons, to further investigate collective synchronization in networks of spiking neurons. We also show that in the limit of slow recurrent synaptic kinetics the QIF-FRE reduce to an equation formally identical to WC equation [cita]. However, as we could observe in the first set of simulations [cita], perturbations applied to uncoupled populations also generated fast oscillatory transients which were not capture by WC equations. Hence, even in this limit, fast fluctuations in external inputs can drive spike synchrony in the network, and consequently the slow synaptic approximation of the QIF-FRE breaks down. This contributes to previously shown results in suggesting that a correct description of spiking networks requires keeping track of the mean subthreshold voltage along with the mean firing rate.

1.3.1 Quadratic Integrate-and-Fire (QIF) model neuron

So far, we have performed numerical simulations using various models of integrate-and-fire neurons and seen similar qualitative behaviors for a wide range of conditions. All these models represent simplified versions of the Hodgkin-Huxley (HH) model with only standard spiking currents. In particular, they are examples of Class I excitability neurons, characterized by the presence of a saddle-node bifurcation on an invariant circle at the transition from quiescence to spiking. Near threshold the spiking dynamics are dominated by the time spent in the vicinity of the saddle-node itself, allowing for a formal reduction in dimensionality from the HH model to a reduced normal-form equation for a saddle-node bifurcation (Ermentrout and Terman, 2010; Ermentrout, 1996; Izhikevich, 2007).

This normal-form is also known as the **Quadratic** integrate-and-fire model which is a specific instance of the generalized integrate-and-fire model [Eq. (1)] in which the voltage dependent function takes the form $f(v) = v^2$. Therefore the QIF neuron represents the canonical model for Class I neurons. The time evolution equation for the membrane potential may be written as (Hansel and Mato, 2001, 2003; Latham et al., 2000)

$$C\frac{du}{dt} = g_L\frac{(u-u_{th})\,(u-u_r)}{u_{th}-u_r} + I_u, \quad (+ \text{ resetting rule}), \tag{1.1}$$

where C is the cell capacitance, g_L is the leak conductance and I_u are input currents. Additional cell parameters are u_{th} and u_r which represent the threshold and resting potentials of the neurons, respectively. As it also happens with the other integrate-and-fire models, the generation of the spike requires a resetting rule. In numerical simulations, once the voltage reaches a given peak value is manually reset to u_r. We can simplify this equation by performing a shift in the membrane potential and rescaling,

$$u' = u - \frac{u_{th}+u_r}{2} \quad \longrightarrow \quad v = \frac{u'}{u_{th}-u_r}, \tag{1.2}$$

reducing the QIF model Eq. (1.1) to

$$\tau_m \frac{dv}{dt} = v^2 + I, \quad (+ \text{ resetting rule}), \tag{1.3}$$

where $\tau_m = C/g_L$ is the membrane time constant, and I are the rescaled (dimensionless) currents

$$I = \frac{I_u}{g_L\,(u_{th} - u_r)} - \frac{1}{4}. \tag{1.4}$$

In the following we will use Eq. (1.3) when referring to the QIF model, and we will denote the (dimensionless) membrane potentials of individual neurons with the letter v.

Notice that the ODE describing the QIF neuron may grow without bound depending on the value of the input currents I. This behavior accounts for the generation of the spike, and therefore requires the use of a resetting rule to return the neuron to the subthreshold regime. Hence, the QIF model exhibits two possible dynamical regimes which depend on the sign of I. If $I < 0$ the neuron is said to be in the excitable regime, whereas for $I > 0$ the neuron is the oscillatory regime. In the excitable regime, an initial condition $v(0) < \sqrt{-I}$ asymptotically approaches the resting potential $-\sqrt{I}$. On the other hand, initial conditions above the excitability threshold, $v(0) > \sqrt{-I}$, lead to an unbounded growth of the membrane potential. Specifically, if $v(0) \gg \sqrt{I}$, then the membrane potential reaches infinity approximately after a time $\tau_m/v(0)$. In numerical simulations, this divergence is usually avoided by implementing a resetting rule by hand. When the membrane potential v reaches a certain peak value $v_p \gg 1$, the neuron is reset to the value $v_r \ll -1$ after a refractory period $\tau_m/v_p + \tau_m/v_p$. Moreover, in the oscillatory regime, $I > 0$, the neuron needs to be reset periodically with an approximate frequency $\nu = \sqrt{I}/(\tau\pi)$, provided $v_p \gg 1$. These dynamical features are summarized in Fig. 1.3.

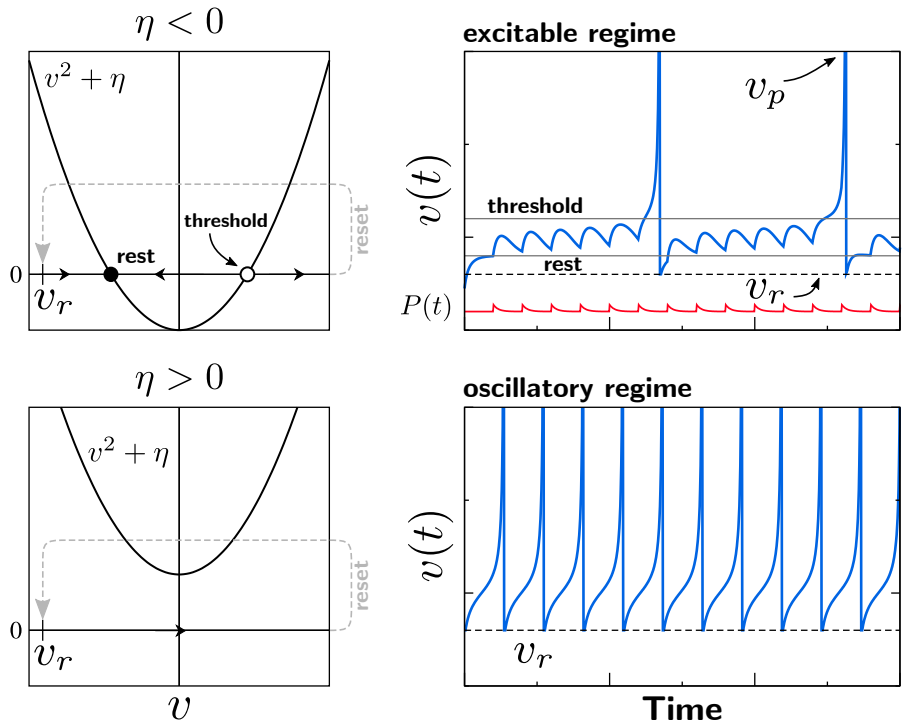

Figure 1.3: Schematic representation of the two possible regimes of the QIF neuron (1.3) with an input current $I = \eta + P(t)$. Top and bottom panels correspond to the excitable and oscillatory regimes, respectively. For each regime, left and right panels show the corresponding phase portrait and a representative time series, respectively. In the top right panel, a time varying external input $P(t)$ is plotted in red, which after some time drives the neuron's voltage across the threshold (○: unstable fix point in the left panel) producing a spike. Then the voltage is reset (gray dashed path in the left panel) to v_r which drives the neuron back to the rest potential (●: stable fix point in the left panel). The effect of any perturbation $P(t)$ in the phase portrait is translated in a vertical shift of the parabola, i.e. excitatory (inhibitory) currents shift the parabola upwards (downwards), with the subsequent displacement of the fix points. In the oscillatory regime there are no fix points and therefore the neuron is firing with a constant frequency proportional to η.

1.3.1.1 Theta neuron

For mathematical analysis of the QIF model, one takes $v_p \to +\infty$ and $v_r \to -\infty$*, which then using the following change of variables

$$v(t) = \tan\left(\frac{\theta(t)}{2}\right), \tag{1.5}$$

the QIF model is transform into a phase model, called the Theta-Neuron model (Ermentrout and Kopell, 1986),

$$\tau_m \frac{d\theta}{dt} = (1 - \cos\theta) + I\,(1 + \cos\theta)\,, \quad \theta \in (-\pi,\ \pi)\,. \tag{1.6}$$

This phase model has an strictly positive Phase Resetting Curve (PRC). Neurons exhibiting such PRCs are known as Type 1 neurons, indicating that (positive) perturbations always produce an advance (and not a delay) of their phase.

Because the theta model is a phase oscillator, it does not properly produce spikes. Therefore, the spike time is normally assumed to take place whenever the phase, $\theta(t)$, crosses $\theta = \pi$. Both models are mathematically equivalent in this limit, and numerical simulations of both models should give similar results.

In the next sections we derive the macroscopic equations for a population of QIF neurons following the work of Montbrió et al. (2015).

1.3.2 Continuity equation for a population of QIF neurons

Let us now consider a population of N all-to-all coupled QIF neurons. The state of the system will be characterized by the neuronal membrane potentials $\{v_i\}_{i=1,\dots,N}$, each obeying Eq. (1.3)

$$\tau_m \frac{dv_i}{dt} = v_i^2 + I_i, \tag{1.7}$$

*In order to mimic this limit in numerical simulations, it is convenient to take $v_r = -v_p$ with $v_p \gg 1$.

where the input currents I_i will account for a constant external current, η_i, and time varying inputs coming from within and outside the population,

$$I_i = \eta_i + JS(t) + P(t). \tag{1.8}$$

The external time varying inputs are denoted as $P(t)$ whereas the recurrent current $Js(t)$ is equal to the synaptic weight J times the mean synaptic activation $s(t)$ due to the firing activity of the population*,

$$S(t) = \frac{1}{N} \sum_{j=1}^{N} \sum_{k} \int_{-\infty}^{t} \alpha_{\tau_s} (t - t') \, \delta \left(t' - t_j^k \right) \, dt'. \tag{1.9}$$

Synaptic activation is the common mean field driving all neurons, which sums the changes in the current due to all the spiking activity occurring prior to time t. Each kth spike emitted by neuron jth is modeled as an instantaneous pulse happening at time $t = t_j^k$ which is represented by a Dirac delta $\delta \left(t - t_j^k \right)$. The pulse is then convoluted with a synaptic kernel α_{τ_s} characterized by the time constant τ_s.

In the limit of infinitely fast synapses, $\tau_s \to 0$, the synaptic activation (1.9) is equivalent to the instantaneous population mean firing rate

$$R(t) = \lim_{\tau_s \to 0} \frac{1}{\tau_s} \frac{1}{N} \sum_{j=1}^{N} \sum_{k} \int_{t-\tau_s}^{t} \delta \left(t' - t_j^k \right) \, dt'. \tag{1.10}$$

1.3.2.1 Continuous formulation

We know exploit the idea of *columnar organization* which states that cortical cells can be grouped into "columns" of neurons with similar properties containing up to several thousand neurons (Hubel and Wiesel, 1968; Lund et al., 2003). This idea allows us to apply the thermodynamic limit in Eqs. (1.7), (1.8) and (1.10), and define the *membrane potential density* function $\rho \left(v | \eta, t \right)$. This approach has been

*For clearer reading, abuse of notation often ignores the integral in the right hand side of Eq. (1.9).

also followed by e.g. Abbott and Van Vreeswijk (1993); Brunel and Hakim (1999); Fusi and Mattia (1999); Brunel (2000); Nykamp and Tranchina (2000); Omurtag et al. (2000). Thus, at time t, the fraction of neurons with membrane potentials between v_0 and $v_0 + \Delta v$ and parameter η is given by

$$\int_{v_0}^{v_0+\Delta v} \rho\left(v|\eta,t\right) dv. \tag{1.11}$$

Additionally, we assume the population to be slightly* heterogeneous by considering a distribution $g(\eta)$ for the external currents ($\eta \in (-\infty,\ \infty)$). Hence, the total voltage density is

$$\int_{-\infty}^{\infty} \rho\left(v|\eta,t\right) g\left(\eta\right) d\eta, \tag{1.12}$$

and bringing back the limit $v_p \to \infty$ and $v_r \to \infty$, the conservation of the number of neurons implies

$$\int_{-\infty}^{\infty} \left(\int_{-\infty}^{\infty} \rho\left(v|\eta,t\right) g\left(\eta\right) d\eta \right) dv = 1, \quad \forall t. \tag{1.13}$$

We may now translate all this [Eqs. (1.7), (1.8), (1.10) and (1.13)] into the continuity equation

$$\frac{\partial \rho}{\partial t} + \frac{\partial}{\partial v} J\left(v|\eta,t\right) = 0, \tag{1.14}$$

where the probability flux $J\left(v|\eta,t\right)$ is the net fraction of neurons with parameter η that crosses the value v per unit time, and is equal to the density of neurons multiplied by the *velocity* of v (right hand side of Eq. (1.7)), that is

$$J\left(v|\eta,t\right) = \frac{1}{\tau_m} \rho\left(v|\eta,t\right) \left(v^2 + \eta + JR + P\right). \tag{1.15}$$

*Neurons are still modeled according to the QIF model neuron, and even though their microscopic parameters may be different, their dynamics are, nonetheless, very similar.

The continuity equation describes the temporal evolution of the distribution of membrane potentials of the neuronal population, and therefore gives a complete dynamical description of the state of the system. However, it still represents a high dimensional system, in which the knowledge of the exact form of the distribution is crucial to obtain a precise description of the macroscopic dynamics.

1.3.3 Dimensionality reduction: Lorentzian Ansatz

What Montbrió et al. discovered, inspired by the work of Ott and Antonsen (2008) and later by Luke et al. (2013); So et al. (2014), was precisely that the distribution of the membrane potentials followed a Lorentzian function (also known as Cauchy distribution). Therefore, by considering the Lorentzian ansatz (LA)

$$\rho\left(v|\eta,t\right)=\frac{1}{\pi}\frac{x\left(\eta,t\right)}{\left[v-y\left(\eta,t\right)\right]^{2}+x\left(\eta,t\right)^{2}} \tag{1.16}$$

the state of the system is completely characterized by **two macroscopic** magnitudes, x and y which have a direct relationship with physically meaningful macroscopic quantities related to the population activity. Similar, but approximate methodology is followed in many other population density models to infer the macroscopic behavior of populations of neurons*.

Notice that the firing rate of the population is just the drift flux $J_{\text{drift}}(v_p|\eta,t)$ through the peak potential v_p (when the spike is emitted). In this particular situation this is written as

$$R\left(\eta,t\right)=\frac{1}{\tau_m}\lim_{v_p\to\infty}\rho\left(v_p|\eta,t\right)\cdot\left.\frac{\partial v}{\partial t}\right|_{v_p}=\frac{x\left(\eta,t\right)}{\pi\tau_m}. \tag{1.17}$$

*Of particular interest is the paper of Amari (1972), where he also obtained two macroscopic quantities related to the width and the mean values of the distribution of membrane potentials

To obtain the **total firing rate** we need to integrate the latter quantity over all possible values of the external current, which gives

$$R\left(t\right)=\frac{1}{\pi\tau_{m}}\int_{-\infty}^{\infty}x\left(\eta,t\right)g\left(\eta\right)d\eta. \tag{1.18}$$

On the other hand, the remaining macroscopic quantity $y\left(\eta,t\right)$ is easily identified with the mean membrane potential, because, by definition, is the center* of the distribution of membrane potentials:

$$y\left(\eta,t\right)=\text{p.v.}\int_{-\infty}^{\infty}\rho\left(v|\eta,t\right)dv, \tag{1.19}$$

and equivalently the **total mean membrane potential** is

$$V\left(t\right)=\int_{-\infty}^{\infty}y\left(\eta,t\right)g\left(\eta\right)d\eta. \tag{1.20}$$

Therefore for a given distribution of external currents $g(\eta)$ the total distribution of membrane potentials can be written as

$$\rho\left(t\right)=\frac{\tau_{m}R(t)}{\left(v-V(t)\right)^{2}+\left(\pi\tau_{m}R(t)\right)^{2}}. \tag{1.21}$$

It is worth commenting on the implications of these preliminary results as compare to the H-FREs [cita]. Here we can see that the mean field approach collapses the infinite-dimensional system into two macroscopic quantities, and hence provides us with a description of the macroscopic dynamics in terms of two variables—x and y, which are related to R and V. In contrast, traditional firing rate models are described only by a single variable, the firing rate.

In Fig. 1.4 an example of the evolution of the network activity under the influence of a time-varying external current, $P(t)$, is shown.

*Moments of the Lorentzian distribution are not well-defined, nevertheless the central value exists and corresponds to its median value, which can be computed by means of the principal value: p.v. $\int_{-\infty}^{\infty}f(x)dx=\lim_{a\to\infty}\int_{-a}^{a}f(x)dx$.

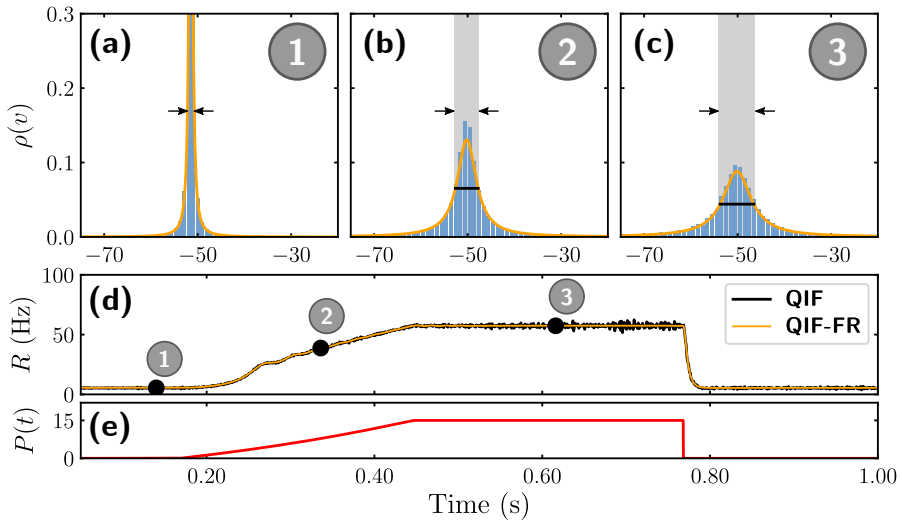

Figure 1.4: Macroscopic observables of the activity, such as the firing rate R in panel (d), are directly related to the membrane potential distribution $\rho(v)$ [Eq. (1.21)]. Panels (a), (b) and (c) show the instantaneous distributions of membrane potentials for three selected instants of the network's evolution depicted in panel (d). The histograms are obtained by numerically simulating a network of $N = 10^4$ QIF neurons subject to a slowly time-varying perturbation $P(t)$, as shown in panel (e). The orange line in panels (a), (b) and (c) is the Lorentzian distribution analytically obtained using the firing rate R and mean membrane potential V from Eqs.[cita]. It can be clearly seen that the full width at half maximum, x (not shown in panel (a)), is related to the firing rate of the neural activity by the simple relation $x = \pi\tau_m R$. In panel (d) the black line corresponds to the firing rate measured from the network of QIF neurons, whereas the orange line has been simulated using Eqs.[cita].

The network consists on an ensemble of $N = 10^4$ heterogeneous uncoupled, $J = 0$, QIF neurons [Eq. (1.7)]. At an approximate time $t = 0.15$ s, a slowly growing perturbation is initiated [Fig. 1.4(e)] which contributes to lowering the firing thresholds of neurons—v_{th} in Fig. 1.3—producing a gradual increase in the firing rate. This change is in activity is very well reflected in the distributions of membrane potentials shown in Figs. 1.4(a), 1.4(b) and 1.4(c), where we can see that for very low firing rates [Fig. 1.4(a)] the distribution is sharply centered at a low value of the membrane potential. As the firing rate is increased, the distribution widens [Figs. 1.4(b) and 1.4(c)] and the center is moved towards the mean threshold potential $v_{th} = -50$ mV. The broadening is intuitively associated with an increase of firing rate, because the drift flux $J_{\text{drift}}(v_p, t)$ at v_p will increase—the density of neurons crossing $v = v_p$ increases. Finally, the conservation of neurons adds a constrain to the normalization of the distribution $\rho(v)$, hence binding $x(t)$ and $y(t)$ in (1.21) together, or equivalently, establishing a functional relationship between $R(t)$ and $V(t)$, respectively.

We may summarize these results in a single conclusion: the correct macroscopic description of spiking networks requires keeping track of the mean subthreshold voltage along with the mean firing rate. We will see that this relation has an important implication when dealing with large rapidly changing input currents, as in this situations the distribution will suffer a sudden kick which, under certain circumstances, will be translated into synchronous leading to macroscopic oscillatory phenomena.

Next, we finally obtain the macroscopic firing rate equations by solving the continuity equation.

1.3.4 Solution to the continuity equation: QIF-FR equations

In order to solve the continuity equation (1.14), we use the LA (1.16) and we obtain the following relation between x and y

$$\frac{\partial}{\partial t}w(\eta,t) = i\left[\eta + JR(t) - w\left(\eta,t\right)^2 + P(t)\right], \tag{1.22}$$

where $w\left(\eta,t\right) \equiv x\left(\eta,t\right) + iy\left(\eta,t\right)$.

- Description of the full QIF model.
- Reduction to the normal form of the saddle-node bifurcation.
- Transfer function of the QIF model (to be used in chapters 2 and 3).

CHAPTER 2

Synchrony-induced modes of oscillation of a neural field model

This work has been developed in collaboration with Daniele Avitabile who performed numerical studies, Alex Roxin and Ernest Montbrió, and it has been published (Esnaola-Acebes et al., 2017)

"Quote"

— Author, Title of Source.

Abstract

We investigate the modes of oscillation of heterogeneous ring-networks of quadratic integrate-and-fire (QIF) neurons with non-local, space-dependent coupling. Perturbations of the equilibrium state with a particular wave number produce transient standing waves with a specific temporal frequency, analogously to those in a tense string. In the neuronal network, the equilibrium corresponds to a spatially homogeneous, asynchronous state. Perturbations of this state excite the network's oscillatory modes, which reflect the interplay of episodes of synchronous spiking with the excitatory-inhibitory spatial interactions. In the thermodynamic limit, an exact low-dimensional neural field model (QIF-NFM) describing the macroscopic dynamics of the network is derived. This allows us to obtain formulas for the Turing eigenvalues of the spatially homogeneous state, and hence to obtain its stability boundary. We find that the frequency of each Turing mode depends on the corresponding Fourier coefficient of the synaptic pattern of connectivity. The decay rate instead is identical for all oscillation modes as a consequence of the heterogeneity-induced desynchronization of the neurons. Finally, we numerically compute the spectrum of spatially inhomogeneous solutions branching from the Turing bifurcation, showing that similar oscillatory modes operate in neural bump states and are maintained away from onset.

2.1 Introduction

Since the pioneering work of Wilson and Cowan (1973), Amari (1974, 1977), and Nunez (1974), continuum descriptions of neuronal activity have become a powerful modeling tool in neuroscience (Ermentrout, 1998; Coombes, 2005; Ermentrout and Terman, 2010; Bressloff, 2012; Coombes et al., 2014; Deco et al., 2008). Given that the number of neurons in a small region of cortex is very large, these descriptions consider neurons to be distributed along a continuous spatial variable and the macroscopic state of the network to be described by a single, space-dependent, firing rate variable. The resulting neural field model (NFM) generally has the form of a continuous first order integro-differential equation, greatly facilitating the computational and mathematical analysis of the dynamics of large neuronal networks.

NFMs do not generally represent proper mathematical reductions of the mean activity of a network of spiking neurons. Nevertheless, NFMs have proven to be remarkably accurate in qualitatively capturing the main types of dynamical states seen in networks of large numbers of asynchronous spiking neurons. For example, it is well known that, in local networks of spiking neurons, differences between excitatory and inhibitory neurons can lead to oscillations (Wilson and Cowan, 1972; Ermentrout, 1994; Brunel and Wang, 2003). The generation of these oscillations does not depend on the spatial character of the network and hence can be observed in non-spatially dependent firing rate models (Ermentrout, 1994). When the pattern of synaptic connectivity depends on the distance between neurons, NFMs show that these differences between excitation and inhibition can lead to the emergence of oscillations and waves (Amari, 1977; Pinto and Ermentrout, 2001). Similar patterns can also be found in NFMs with spatially dependent delays —modeling the effect of the finite velocity propagation of action potentials (Wilson and Cowan, 1973; Jirsa and Haken, 1997)— as a great deal of theoretical work indicates (see e.g. Coombes et al., 2003; Atay and Hutt, 2004; Coombes and Laing, 2009; Zhang, 2007; Hutt, 2008; Touboul, 2012; Veltz, 2013; Dijkstra et al., 2015).

In some cases the spatio-temporal dynamics of NFMs has been directly compared to that observed in analogous networks of spiking neurons (Roxin et al., 2005; Battaglia et al., 2007; Roxin and Montbrió, 2011). In this work it was found that non-space-dependent delays predict the existence of many of the spatiotemporal patterns observed in asynchronous networks of spiking neurons with nonlocal, space-dependent interactions. The success of NFMs in describing these patterns depends crucially on the spiking activity being highly asynchronous. In fact, it is well known that neural field descriptions fail to describe states characterized by a high degree of spike synchronization (see e.g Schaffer et al., 2013).

Here we report a spatiotemporal dynamical feature of heterogeneous networks of spiking neurons with nonlocal interactions that, to the best of our knowledge, have been so far unexplored. We show that ring networks of spiking neurons display a number of discrete modes of oscillation, resembling those of a tense string. These modes are exclusively due to transient episodes of synchronous spiking and not due to the different time scales between excitation and inhibition or to the presence of any propagation or synaptic delay.

Traditional NFMs do not describe these synchrony-induced oscillations. Therefore, to investigate and characterize them, we apply a recent method to derive the firing rate equations of a globally coupled heterogeneous population of quadratic integrate-and-fire (QIF) neurons (Montbrió et al., 2015). This method, based on the so-called Ott-Antonsen theory (Ott and Antonsen, 2008, 2009; Ott et al., 2011), leads to an exact macroscopic description of the network in terms of two macroscopic variables: the mean firing rate and the mean membrane potential. The resulting mean-field model exactly describes any state of the system, including synchronous states. Here we extend the local firing rate model in (Montbrió et al., 2015), to include nonlocal, instantaneous interactions. The resulting neural field model for heterogeneous QIF neurons (QIF-NFM) clearly displays the synchrony-induced oscillatory modes observed in simulations of spiking neurons. We then thoroughly investigate the QIF-NFM by means of both a

linear and nonlinear stability analysis of the spatially homogeneous state. The analysis reveals the presence of an infinite number of oscillation modes, linked to the Fourier components of the spatial pattern of synaptic connections. The analysis also shows that all modes decay to the unpatterned state with the same rate, which depends on the degree of heterogeneity in the network. Finally, we investigate the spectrum of the spatially inhomogeneous solutions of the QIF-NFM and find similar oscillatory modes also linked to transient episodes of spike synchronization.

2.2 Synchrony-induced modes of oscillation in Networks of QIF Neurons

Figure (2.1, a) shows a schematic representation of the spiking neuron network under investigation. The model consists of N excitatory (red triangles) and N inhibitory (blue circles) neurons evenly distributed in a ring and characterized by the spatial discrete variables $\phi_j \in [-\pi, \pi)$ with $\phi_j = \frac{2\pi j}{N} - \pi,\ j = 1, \ldots, N$. Any neuron in the network interacts with all the other neurons via the distance-dependent coupling function $J^{e,i}_{jk} = J^{e,i}(|\phi_j - \phi_k|)$, where indices e, i denote excitatory and inhibitory connections, respectively. The synaptic projections of the jth excitatory and inhibitory neurons (located at ϕ_j) to other two nearby neurons are also schematically represented in Figure (1,a).

The ring architecture of the network allows one to express the excitatory and inhibitory connectivity patterns in Fourier series as

$$J^{e,i}(\phi) = J^{e,i}_0 + 2\sum_{K=1}^{\infty} J^{e,i}_K \cos(K\phi). \tag{2.1}$$

Figure (2.1,b) shows a particular synaptic connectivity pattern in which excitatory neurons form strong, short-range connections, whereas inhibitory projections are weaker and wider. The state of the excitatory (e) and inhibitory (i) neurons is determined by the (dimensionless) membrane potentials $\{v^{e,i}_j\}_{j=1,\ldots,N}$, which are modeled using the

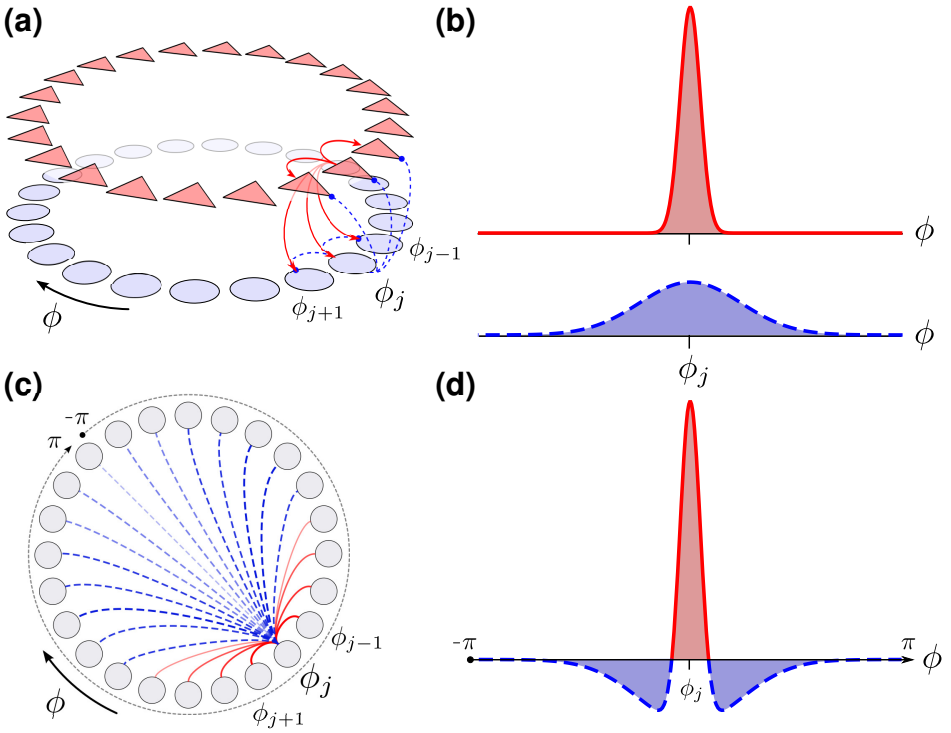

Figure 2.1: Schematic representation of the ring network and coupling architecture under study. Panel (a) shows N excitatory (red triangles) and N inhibitory (blue circles) neurons arranged on a ring. The location of neurons is parameterized by the angular variable $\phi_j = \frac{2\pi j}{N} - \pi$, $j = 1, \ldots, N$. Red (solid) and blue (dashed) lines indicate synaptic connections between neuron pairs (ϕ_j, ϕ_k). An example of the excitatory and inhibitory space-dependent connectivity kernels Eqs. (2.1) are shown in panel (b) where the abscissa represents the distance $|\phi_k - \phi_j|$ between neurons j and k. Panel (c) represents an effective model in which pairs of excitatory/inhibitory neurons located at a certain location ϕ_k are modeled as single neurons. The effective pattern of synaptic connectivity is obtained subtracting the inhibitory pattern from the excitatory one, as show in panel (d).

Quadratic Integrate and Fire (QIF) model Ermentrout and Kopell (1986); Izhikevich (2007)

$$\tau \frac{dv_j^{e,i}}{dt} = (v_j^{e,i})^2 + I_j^{e,i}, \quad (+ \text{ resetting rule}). \tag{2.2}$$

where τ is the cell's membrane time constant and v_r and v_p correspond to the reset and peak potentials of the QIF neurons, respectively —in numerical simulations we consider $\tau = 20$ ms. The QIF neuron has two possible dynamical regimes depending on the (dimensionless) input current $I_j^{e,i}$. If $I_j^{e,i} < 0$, the neuron is in the excitable regime, while for $I_j^{e,i} > 0$ the neuron is in the oscillatory regime. In the excitable regime, an initial condition $v_j^{e,i}(0) < \sqrt{-I_j^{e,i}}$, asymptotically approaches the resting potential $-\sqrt{-I_j^{e,i}}$. On the other hand, initial conditions above the excitability threshold, $v_j^{e,i}(0) > \sqrt{-I_j^{e,i}}$, lead to an unbounded growth of the membrane potential. Specifically, if $v_j^{e,i}(0) \gg \sqrt{I_j^{e,i}}$, then the membrane potential reaches infinity approximately after a time $\tau / v_j^{e,i}(0)$. In practice, to avoid this divergence, we consider the following resetting rule: When the neuron's membrane potential $v_j^{e,i}$ reaches a certain peak value $v_p \gg 1$, the neuron is reset to a the new value $v_r = -v_p$ after a refractory period $2\tau/v_p$. On the other hand, if $I_j^{e,i} > 0$, then the neuron is in the oscillatory regime and needs to be reset periodically. If $v_p \gg 1$, the frequency of the oscillatory neurons is approximately $f_j = \sqrt{I_j}/(\tau\pi)$. Finally, the current $I_j^{e,i}$ is defined as

$$I_j^{e,i} = \eta_j^{e,i} + \tau S_j^e(t) + \tau S_j^i(t) + P_j^{e,i}(t). \tag{2.3}$$

Here, $\eta_j^{e,i}$ is a constant external current, which varies from neuron to neuron. The terms $P^{e,i}(t)$ are time-varying common inputs, and $S_j^{e,i}(t)$ are the mean excitatory (positive) and inhibitory (negative) synaptic activities representing all the weighted inputs received by

neuron j due to spiking activity in the network:

$$S_j^{e,i}(t) = \pm \sum_{k=1}^{N} \frac{J_{jk}^{e,i}}{2\pi N} \sum_{l \backslash t_k^l < t} \frac{1}{\tau_s} \int_{t-\tau_s}^{t} dt' \delta^{e,i}(t' - t_k^l), \qquad (2.4)$$

where τ_s represents the synaptic processing time and t_k^l is the time of the lth spike of the excitatory/inhibitory kth neuron. Positive and negative signs correspond to S_j^e and to S_j^i, respectively.

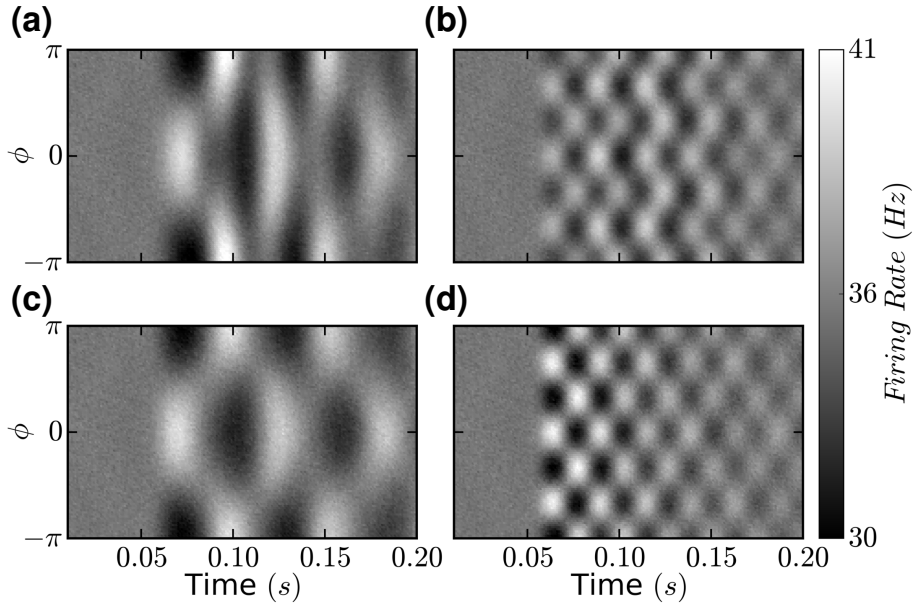

Figure 2.2: Transient episodes of spike synchrony in heterogeneous ring networks of $N = 2.5 \cdot 10^5$ excitatory and $N = 2.5 \cdot 10^5$ inhibitory QIF neurons, Eqs. (2.2) and (2.3), as a result of spatially inhomogeneous perturbations applied at time $t = 0.05$ s. In Panels (a) and (b) only excitatory neurons are perturbed. In panels (c) and (d) all neurons are perturbed. In panels (a) and (c) the perturbation has wave number $K = 1$; in panels (b) and (d) the perturbation has wave number $K = 3$. Other parameters are $\Delta = 1$, $\tau = 20$ ms, and $\bar{\eta} = 5$. All Fourier components of the connectivity Eq. (2.1) were $J_K^{e,i} = 0$, except $J_0^e = 23$, $J_1^e = 10$, $J_2^e = 7.5$, $J_3^e = -2.5$, $J_0^i = 23$.

We performed numerical simulations of the QIF model Eqs. (2.2) and (2.3) for a network of heterogeneous neurons, see Figure 2.2, and Appendix 2.D for details of the numerical simulations. In all cases, the system is initially at a spatially homogeneous state (SHS). At time $t = 50$ ms, a brief (10 ms) and small current pulse P_j^e is applied either to only excitatory neurons (panels a, b) or to both excitatory and inhibitory neurons. The left and right panels show perturbations of the first spatial modes, respectively —see Appendix D for the specific form of the perturbations. Note that, after the perturbation, the system decays to the homogeneous state showing oscillations, which resemble standing waves. Note that the frequency of these oscillations is different for each mode, while the decay rate is similar in the two cases. We also performed simulations of networks of QIF neurons (i) with quenched Gaussian heterogeneity (ii) subject to independent Gaussian noise processes, and found similar results (not shown). To the best of our knowledge, these oscillations have not yet been investigated in the literature.

2.3 Neural Field model for quadratic integrate and fire neurons

In the following, we aim to investigate the nature and origin of the spatiotemporal patterns shown in Figure 2.2. To analyze them, we derive the NFM corresponding to the thermodynamic ($N \to \infty$) and continuum limits of the network of QIF neurons [Eqs. (2.2) and (2.3)]. In additon we also take the limit $v_p \to \infty$, so that the QIF model (2.2) is equivalent to the so-called theta-neuron model (Ermentrout and Kopell, 1986; Izhikevich, 2007). This leads to an exact neural field model for a network of QIF neurons (QIF-NFM). The detailed derivation is performed in Appendix 2.A, and closely follows that of Montbrió et al. (2015). The reduction in dimensionality is achieved considering that the currents $\eta^{e,i}$ —which, after performing the thermodynamic limit, become continuous random variables— are distributed according

to a Lorentzian distribution of half-width Δ and centered at $\bar{\eta}$,

$$g(\eta^{e,i}) = \frac{\Delta}{\pi} \frac{1}{(\eta^{e,i} - \bar{\eta})^2 + \Delta^2}. \tag{2.5}$$

The QIF-NFM is

$$\begin{aligned} \tau \frac{\partial R^{e,i}}{\partial t} &= \frac{\Delta}{\pi\tau} + 2R^{e,i}V^{e,i}, & \text{(2.6a)} \\ \tau \frac{\partial V^{e,i}}{\partial t} &= (V^{e,i})^2 + \bar{\eta} - (\pi\tau R^{e,i})^2 + \tau S(\phi) \\ &\quad + P^{e,i}(\phi, t). & \text{(2.6b)} \end{aligned}$$

and exactly describes the time evolution of the mean firing rate $R^{e,i}(\phi)$ and the population's mean membrane potential $V^{e,i}(\phi)$ of the excitatory and inhibitory populations at any location ϕ of the ring —to facilitate the notation we have avoided explicitly writing the dependence of these variables on ϕ. In the limit of instantaneous synapses, $\tau_s \to 0$ in Eqs. (2.4), the excitatory and inhibitory contributions of the mean field $S(\phi) = S^e(\phi) + S^i(\phi)$ reduce to $S^{e,i}(\phi) = \pm \frac{1}{2\pi} \int_{-\pi}^{\pi} J^{e,i}(\phi - \phi') R^{e,i}(\phi') d\phi'$.

2.3.1 Effective QIF-NFM

The analysis of the QIF-NFM Eq. (2.6) is greatly simplified considering that excitatory and inhibitory neurons have identical single-cell properties. This scenario is schematically represented in Figs. 2.1(c) and 2.1(d). If we set $P^e(\phi, t) = P^i(\phi, t) = P(\phi, t)$, and restrict our attention to solutions of Eqs. (2.6) satisfying $R^e(\phi, t) = R^i(\phi, t) \equiv R(\phi, t)$ and $V^e(\phi, t) = V^i(\phi, t) \equiv V(\phi, t)$, then we obtain an effective QIF-NFM in variables R and V,

$$\begin{aligned} \tau \frac{\partial R}{\partial t} &= \frac{\Delta}{\pi\tau} + 2RV, & \text{(2.7a)} \\ \tau \frac{\partial V}{\partial t} &= V^2 + \bar{\eta} - (\pi\tau R)^2 + \tau S(\phi) + P(\phi, t). & \text{(2.7b)} \end{aligned}$$

In this case, the mean field reduces to

$$S(\phi) = \frac{1}{2\pi} \int_{-\pi}^{\pi} \left[J_0 + 2 \sum_{K=1}^{\infty} J_K \cos(K(\phi' - \phi)) \right] R(\phi') d\phi', \qquad (2.8)$$

with the new Fourier coefficients J_K, which are related to those in Eq. (2.1) as $J_K = J_K^e - J_K^i$, with $K = 0, 1, \ldots$, see Fig.2.1(d). Solutions to Eqs. (2.6) need not satisfy the condition $R^e = R^i$ and $V^e = V^i$, but the reduced system Eqs. (2.7) captures the mechanism behind the oscillatory behavior observed in the model. Note that, in Figs. 2.2(a) and 2.2(b), we perturbed the (SHS) of the system [Eqs. (2.2) and (2.3)] using a current pulse to all excitatory neurons. The resulting dynamics is only captured by the full system [Eqs. (2.6)] and not by the effective neural field [Eqs. (2.7)]. However, we next show that the existence of the spatial oscillatory modes observed in Fig.2.2 is exclusively linked to the dynamics in the reduced manifold defined by Eqs. (2.7) and (2.8).

2.3.2 SHS and their stability: Synchrony-induced modes of oscillation

In the following we investigate the stability of the stationary SHS of the QIF-NFM against spatial perturbations. The detailed linear stability analysis of both the complete model [Eqs. (2.6)], and the reduced one [Eqs. (2.7)] are provided in Appendix 2.B.

In absence of external inputs, $P(\phi, t) = 0$, the steady states of Eqs. (2.7)—and also of Eqs. (2.6)—satisfy $V_*(\phi) = -\Delta/[2\pi\tau R_*(\phi)]$, and

$$R_*(\phi) = \Phi\left(\bar{\eta} + \tau S_*(\phi)\right) \qquad (2.9)$$

with $\Phi(x) = \sqrt{x + \sqrt{x^2 + \Delta^2}}/(\sqrt{2}\pi\tau)$. In Eq. (2.9), the term $S_*(\phi)$ is the mean field [Eq. (2.8)] evaluated at $R_*(\phi)$. For SHS, the mean field [Eq. (2.8)] becomes spatially independent, $S_*(\phi) = S_* = J_0 R_*$, and Eq. (2.9) becomes a quartic equation for the variable R_*. To

further simplify the analysis, hereafter we consider parameter ranges where Eq. (2.9) has a single positive root. Accordingly, we consider a balanced kernel, $J_0 = 0$ so that Eq. (2.9) has $S_* = 0$ and explicitly determines the value of the fixed point R_*.

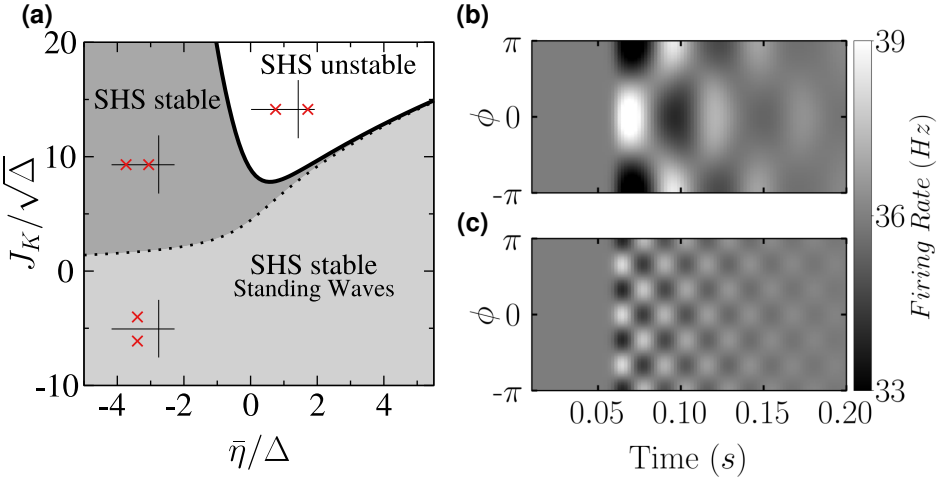

Figure 2.3: (a) Phase diagram of Eqs. (2.7) (with $J_0 = 0$) showing the regions of stability of the SHS, determined by the eigenvalues Eq. (2.10). Spatial perturbations of wave number $K > 0$ show oscillatory and nonoscillatory decay to the spatially homogeneous state in the light-shaded and dark-shaded regions of the diagram, respectively. The eigenvalues $\lambda_{K\pm}$ associated with the Kth mode are schematically represented in the complex plane (red crosses) for the three qualitatively different regions of the phase diagram. Right panels show the response of the Eqs. (2.7) with $J_1 = 10$, $J_2 = 7.5$, $J_3 = -2.5$ and $J_K = 0$ ($K \neq 1, 2, 3$), $\bar{\eta} = 4.5$, $\Delta = 1$, and $\tau = 20$ ms, to a perturbation of the (b) $K = 1$ and (c) $K = 3$ spatial modes. Both perturbations produce standing waves with frequency and decay rate described by Eqs (2.10). In the white region, limited by the curve Eq. (2.11), these perturbations grow and lead to a bump state (BS) with K bumps (see Fig. 2.4).

The steady states of the SHS of Eq.(2.7) coincide with those of a single population of neurons (Montbrió et al., 2015). However, the stability of the SHS of the QIF-NFM to inhomogeneous perturbations depends on the spatial character of the connectivity kernel Eq. (2.1). The linear stability analysis of the SHS gives a countably infinite set

of eigenvalues associated to the stability of perturbations with wave number* K.

$$\lambda_{K\pm} = -\frac{\Delta}{\pi\tau^2 R_*} \pm 2\pi R_* \sqrt{\frac{J_K}{2\pi^2\tau R_*} - 1},\ (K = 0, 1, 2\dots) \qquad (2.10)$$

This equation is the main result of this work, and explains the synchronization patterns shown in Fig. 2.2. Note that the eigenvalues Eq. (2.10) may be real or complex, indicating nonoscillatory or oscillatory dynamics of the evolution of perturbations of wave number K, respectively. In particular, perturbations of any given spatial mode K are oscillatory if the condition $J_K < 2\pi^2\tau R_*$ is fulfilled. Notably, all complex eigenvalues have the same decay rate to the SHS, since $\mathrm{Re}(\lambda_{K\pm}) = -\Delta/(\pi\tau^2 R_*)$ for all of them. Specifically, the decay rate is proportional to the degree of quenched heterogeneity Δ. This reflects the fact that the decay in the oscillations is in fact a desynchronization mechanism due to the distribution of inputs that the cells receive.

Substituting Eq. (2.9) with $J_0 = 0$ into Eq. (2.10), it is straightforward to find the boundary

$$J_K^o = \sqrt{2}\pi\sqrt{\bar{\eta} + \sqrt{\bar{\eta}^2 + \Delta^2}}, \qquad (2.11)$$

separating the parameter space into regions where standing waves of wave number K are, or are not, observed. This boundary is depicted with a dotted line in the phase diagram Fig. (2.3), together with a schematic representation of the location of the eigenvalues $\lambda_{K\pm}$ in the complex plane (red crosses, see also Fig.2.5(a)).

A given oscillatory mode K has an associated frequency $\nu_K = 1/(2\pi)|\mathrm{Im}(\lambda_{K\pm})|$, which differs from one another depending on the

* The stability analysis of the original Eqs. (2.6) gives two additional complex eigenvalues for each oscillatory mode K. These eigenvalues are degenerated and are associated to the oscillatory modes of the uncoupled neuronal system, that is they coincide with (2.10) with $J_K^{e,i} = 0$. Additionally, due to the translational invariance of the SHS solutions, each of the eigenvalues Eq. (2.10) is two-times degenerated, corresponding to even and odd perturbations. See Appendix 2.B for the detailed linear stability analysis of the QIF-NFM Eqs. (2.6).

corresponding Fourier coefficients J_K of the patterns of synaptic connectivity Eq. (2.1). Therefore, spatial perturbations of wave number K produce standing waves of neural activity of frequency ν_K. Locally excitatory coupling $J_K > 0$ slows down these oscillations and eventually suppresses them, whereas locally inhibitory coefficients $J_K < 0$ are able to generate arbitrarily fast oscillations (in particular, note that all modes with $J_K = 0$ are oscillatory with frequency $\nu = R_*$, which coincides with the mean firing rate of the uncoupled neurons).

Indeed, in Fig. 2.2(d), a perturbation of wave number $K = 3$ produced standing waves, since J_3 was negative. The frequency of these oscillations was fast compared to that of Fig. 2.2(c), where the exited mode was the first one $K = 1$ and given that the J_1 was positive. However, note that in both cases the decay to the SHS is similar, as predicted by the eigenvalues Eq. (2.10). This indicates that the desynchronization process occurs faster when the diversity Δ of neurons is increased, and this process does not depend on the oscillation mode being excited. Finally, in Figs. 2.3(b) and 2.3(c) we show numerical simulations of the QIF-NFM [Eq. (2.7)] using the same parameters as those of Fig. 2.2(c) and 2.2(d), and the agreement is good.

2.3.3 Turing bifurcation and nonlinear stability of the SHS

As J_K is increased, the frequency ν_K of a given oscillatory mode decreases and eventually it ceases to oscillate. Further increases in J_K may destabilize the homogeneous state, via a pattern-forming (Turing) bifurcation. This instability leads to states with spatially modulated firing rate, sometimes referred to as Bump States (BS). Substituting the fixed point (2.9) in Eq. (2.10), and imposing the condition of marginal stability $\lambda_{K+} = 0$, we find the stability boundaries

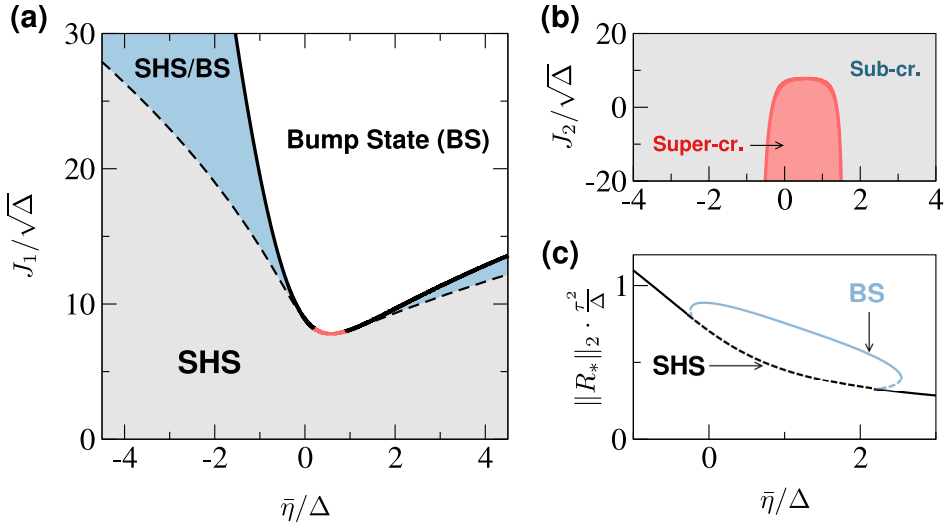

Figure 2.4: (a) Phase diagram of the QIF-NFM [Eqs. (2.7)] with $J_2 = 7.5$, $J_3 = -2.5$, $J_K = 0$ for $K > 3$, and $\Delta = 1$. Solid line: Supercritical [red (gray)] and Subcritical (black) Turing bifurcation boundary Eq. (2.12). Dashed lines: saddle-node bifurcation of bumps (numerical). (b) Diagram —obtained using a weakly nonlinear analysis— showing the regions where the Turing bifurcation is supercritical or subcritical for $J_1 = 10$, $J_3 = -2.5$, and $J_K = 0$. (c) Bifurcation diagram (rescaled) $\|R_*\|_2 = (2\pi)^{-1} \int_{-\pi}^{\pi} |R_*(\phi)|^2 d\phi$ vs. $\bar{\eta}$, for $J_1 = 10$. Solid/dashed black lines: stable/unstable SHS. Solid/dashed blue lines: stable/unstable bump states (BS).

corresponding to a K-spatial mode

$$J_K^T = 2\pi \sqrt{\frac{2\bar{\eta}^2 + 2\Delta^2}{\bar{\eta} + \sqrt{\bar{\eta}^2 + \Delta^2}}}. \tag{2.12}$$

The Turing bifurcation boundary, Eq. (2.12), corresponds to the solid line in Figs. 2.3(a) and 2.4(a). Additionally, in Appendix 2.C, we conducted a weakly nonlinear analysis and derived the small-amplitude equation [Eq. (2.C.20)] corresponding to the bump solution bifurcating from the SHS. The amplitude equations determine if the Turing bifurcation is supercritical, or if it is subcritical and bistability between

SHS and bump states is expected to occur. The results of this analysis are summarized in Fig. 2.4(b).

In addition, we performed numerical simulations of the QIF-NFM (2.7) and indeed found coexistence of SHS and bump states in the blue-shaded regions limited by solid and dashed curves in Fig. 2.4(a). These lines meet at two codimension-2 points (where the Turing bifurcation line changes color) that agree with the results of the weakly nonlinear analysis. Moreover, we computed numerically a bifurcation diagram of the NFM, using the spectral method developed in (Rankin et al., 2014) and available with (Avitabile, 2016). The results, presented in Fig. 2.4(c) confirm that the unstable BS bifurcates subcritically for the SHS. The unstable BS then meets a stable BS —solid blue (light gray) line— at a fold bifurcation.

2.3.4 Synchrony-induced transient oscillations in bump states

To investigate whether the synchrony-induced oscillatory modes are also present in the stationary BS, we computed their spectrum. The gray points in Fig. 2.5(a) show the spectrum of the unstable Bump near the subcritical Turing bifurcation of wave number $K = 1$. Additionally, the red crosses in Fig. 2.5(a) are the eigenvalues of the SHS state Eq. (2.10). The profile of the unstable bump is only very weakly modulated, see Fig. 2.5(c), and hence the spectrum of the BS is very close to that of the SHS, given by the eigenvalues λ_K. All these eigenvalues are complex, except two real eigenvalues, which correspond to the $K = 1$ mode. One of these eigenvalues is negative and the other is very close to zero and positive, indicating that the SHS is unstable.

Additionally, it is important to note that in Fig. 2.5 we have taken $J_K = 0$ for all K except for $K = 1, 2, 3$, and hence there is an infinite number of eigenvalues (λ_0 and $\lambda_{4,5,\ldots}$) that are all complex and identical. In Fig. 2.5(a) the eigenvalues of the unstable BS seem to form a continuous band precisely around these infinitely degenerated eigenvalues and their complex conjugates. These continuous bands

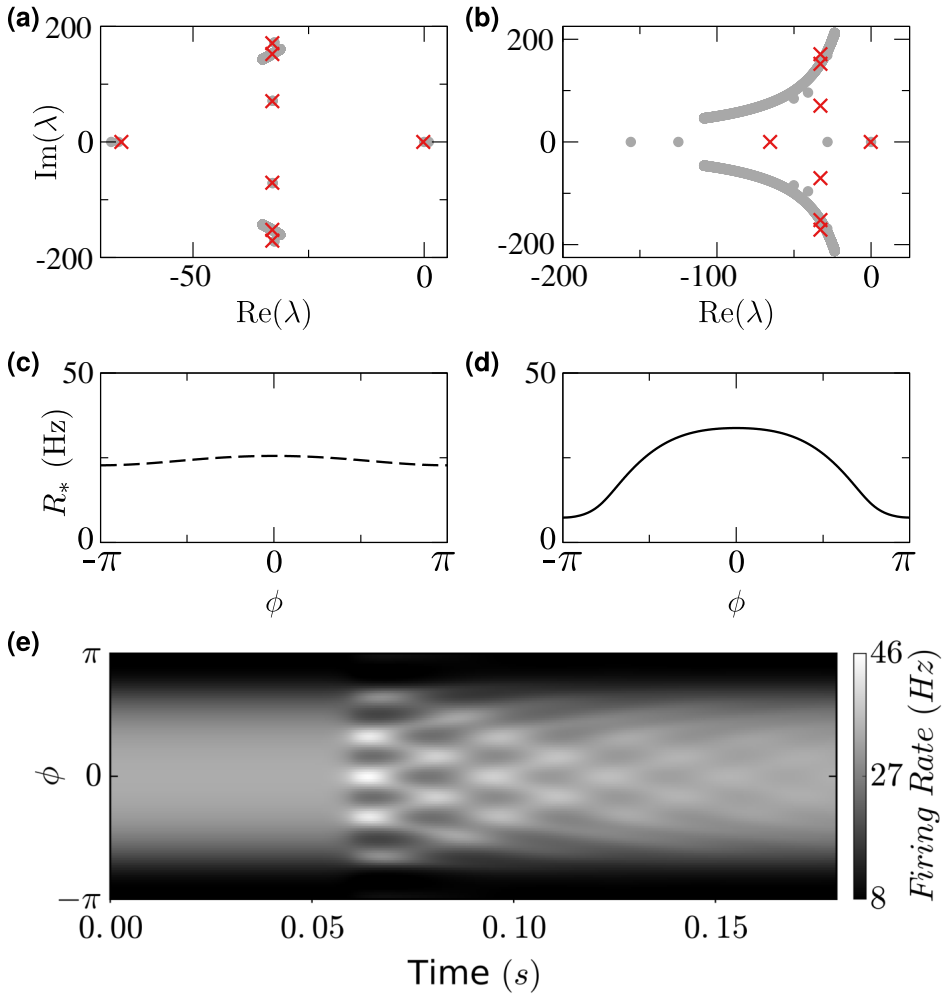

Figure 2.5: Spectrum [(a) and (b)] and firing rate profiles [(d) and (c)] of an unstable [(a) and (c)] and stable [(b) and (d)] bump states of the QIF-NFM [Eqs. (2.7)]. In panels (a) and (b) the eigenvalues Eq. (2.10) are superimposed with red crosses. Panel (e) shows a numerical simulation of the BS of panel (d). At $t = 0.05$ s, a perturbation of wave number $K = 6$ is applied. Parameters are $J_0 = 0$, $J_1 = 10$, $J_2 = 7.5$, $J_3 = -2.5$, $J_K = 0$ for $K > 3$, $\Delta = 1$, $\tau = 20$ ms. Panels (a) and (c): $\bar{\eta} = 2.2120$; panels (b), (d) and (e): $\bar{\eta} = 2.1828$.

grow in size as one moves away from the Turing bifurcation, as it can be seen in the spectrum of the stable bump depicted in Fig. 2.5(b) —here red crosses also correspond to the eigenvalues of the SHS state Eq. (2.10). These results show that all the complex eigenvalues linked to the oscillatory modes of the SHS remain complex, suggesting that, in general, similar synchronization-induced oscillations may be present in stationary, spatially inhomogeneous neural patterns.

Finally, to illustrate this, in Fig. 2.5(e) we performed a numerical simulation of the QIF-NFM Eqs. (2.7), and perturbed the BS shown in Fig.2.5(d) with a spatially inhomogeneous perturbation corresponding to the mode ($K = 6$). The perturbation decays to the BS showing a pattern that resembles that of Figs. (2.2). However here, the regions of the ring with the maximum values of R_* —around $\phi = 0$, in Figs. 2.2(d) and 2.2(e)— oscillate at high frequencies and these oscillations slow down as $\phi \to \pm\pi$. The spectrum of the stable BS Fig. 2.5(b) also indicates that the decay of the fast oscillations (located at the central part of the bump, $\phi = 0$) is slow compared to that of the slow oscillations.

2.4 Conclusions

We have reported the existence of a class of oscillatory modes in spatially distributed networks of heterogeneous spiking neurons. These modes of oscillation reflect the transient episodes of spike synchronization among the neurons and are not captured by traditional NFMs.

To investigate these oscillation modes we derived a novel NFM for QIF neurons [Eqs. (2.6)]. Alternately, and invoking the Ott-Antonsen theory for populations of pulse-coupled theta neurons (Luke et al., 2013; So et al., 2014), Laing (2014) recently derived a NFM that is equivalent to the effective QIF-NFM. In Laing's work—like in other recent related papers on pulse-coupled oscillators (Pazó and Montbrió, 2014; O'Keeffe and Strogatz, 2016; Chandra et al., 2017; Coombes and Byrne, 2019; Byrne et al., 2017; Gallego et al., 2017)— the resulting

low-dimensional description is in terms of the complex Kuramoto order parameter. In contrast, the mean field description adopted here (in terms of mean firing rates and membrane potentials) greatly simplifies the analysis, allowing us to analytically investigate the linear and nonlinear stability of the spatially homogeneous states of the QIF-NFM.

This analysis reveals two important features: (i) The frequency of each oscillation mode only depends on the corresponding Fourier coefficient of the synaptic pattern of connectivity, and (ii) the decay rate is exactly the same for all modes and is due to a desynchronization mechanism which depends on the degree of quenched heterogeneity. We also numerically investigated networks of identical QIF neurons subject to noise and found similar results (not shown). In this case, the desynchronization reflects an underlying phase diffusion proportional to the noise strength. Finally, we investigated the existence and stability of bump states, which bifurcate from the spatially homogeneous states via Turing bifurcations. The spectrum of such bump states has a continuous part off the real axis, indicating that similar synchronization-induced oscillatory modes also operate in neural bump states.

Interesting directions of further study are the analysis of the QIF-NFM [Eq. (2.6)] considering different membrane time constants τ, (or different main currents $\bar{\eta}$) for excitatory and inhibitory neurons. As proved recently (Avitabile et al., 2017), NFMs with time-scale separation display a rich variety of robust spatiotemporal patterns, which may also be supported by our model. Also, recent work has been done to extend the local firing rate equations derived in (Montbrió et al., 2015) to include fixed synaptic delays (Pazó and Montbrió, 2016) and synaptic kinetics (Ratas and Pyragas, 2016; Devalle et al., 2017)—see also (Coombes and Byrne, 2019; Byrne et al., 2017). This work shows that time delays due to synaptic processing generally lead to the emergence of self-sustained oscillations due to collective synchronization. Extending the QIF-NFM [Eq. (2.6)] to account for the synaptic time delays caused by synaptic processing may lead

to spatiotemporal phenomena not previously observed in traditional NFMs.

Acknowledgments

J.M.E.-A. and E.M. acknowledge support by European Union's Horizon 2020 research and innovation programme under the Marie Skłodowska-Curie Grant No. 642563. J.M.E.-A. and E.M. acknowledge the projects grants from the Spanish Ministry of Economics and Competitiveness, Grants No. PSI2016-75688-P and No. PCIN-2015-127. A.R. acknowledge a project grant from the Spanish ministry of Economics and Competitiveness, Grant No. BFU2012-33413. A.R. has been partially funded by the CERCA progam of the Generalitat de Catalunya. D.A. was partially supported by the EPSRC Grant No. EP/P510993/1 (United Kingdom).

Chapter Appendices

2.A Derivation of the QIF neural field model (QIF-NFM)

Our derivation closely follows that of (Montbrió et al., 2015), but it needs to be extended to include the spatial dimension. Similar extensions from a single population of phase oscillators to a one-dimensional, spatially distributed network with nonlocal coupling have been done in (Laing, 2014, 2015, 2016b,a, 2009; Omel'chenko, 2013; Omel'chenko et al., 2014; Kawamura, 2014).

Considering the thermodynamic limit $N \to \infty$, we can drop the indexes in Eqs. (2.2) and (2.3) and define the density function $\rho^{e,i}(v^{e,i}|\eta^{e,i}, t, \phi)$ such that $\rho^{e,i}(v^{e,i}|\eta^{e,i}, t, \phi)dv^{e,i}d\eta^{e,i}d\phi$ describes the fraction of neurons located between ϕ and $\phi + d\phi$, with membrane potentials between $v^{e,i}$ and $v^{e,i} + dv^{e,i}$ and parameters between $\eta^{e,i}$ and $\eta^{e,i} + d\eta^{e,i}$ at time t. Accordingly, parameter $\eta^{e,i}$ becomes now a continuous random variable with probability density function $g(\eta^{e,i})$. For the sake of simplicity, we assume identical distributions for both excitatory and inhibitory populations $g\left(\eta^{e,i}\right) = g\left(\eta\right)$. The total voltage density at location ϕ and time t is given by $\int_{-\infty}^{\infty} \rho^{e,i}(v^{e,i}|\eta, t, \phi)\ g(\eta)\ d\eta$.

Conservation of the number of neurons at each ϕ value is described by the continuity equation

$$\partial_t \rho^{e,i} = -\partial_v \left[\left(\left(v^{e,i}\right)^2 + \eta + \tau S(\phi, t) + P^{e,i}(\phi, t) \right) \rho^{e,i} \right],$$

where we have explicitly included the velocity given by Eqs. (2.2) and (2.3) and $S\left(\phi, t\right) = S^e\left(\phi, t\right) + S^i\left(\phi, t\right)$ represents the total synaptic activity. Next we invoke the Ott-Antonsen theory (Ott and Antonsen, 2008), by means of the Lorentzian Ansatz (LA) (Montbrió et al., 2015)

$$\rho^{e,i}(v^{e,i}|\eta, t, \phi) = \frac{1}{\pi} \frac{x^{e,i}(\phi, \eta, t)}{\left[v^{e,i} - y^{e,i}(\phi, \eta, t)\right]^2 + x^{e,i}(\phi, \eta, t)^2}, \qquad (2.A.1)$$

which solves the continuity equation. The width $x^{e,i}(\phi,\eta,t)$ of the LA is related to the firing rate $R^{e,i}$ of the neural populations. Indeed, for each η value at time t, $R^{e,i}(\phi,\eta,t)$ can be evaluated noting that neurons fire at a rate given by the probability flux at infinity: $R^{e,i}(\phi,\eta,t) = \rho^{e,i}(v^{e,i}\to\infty|\eta,t,\phi)\dot{v}^{e,i}(v^{e,i}\to\infty|\eta,t,\phi)$. The limit $v^{e,i}\to\infty$ on the right-hand side of this equation can be evaluated within the LA and gives: $x^{e,i}(\phi,\eta,t) = \pi\tau R^{e,i}(\phi,\eta,t)$. The total firing rate at a particular location ϕ of the ring is then

$$R^{e,i}(\phi,t) = \frac{1}{\tau\pi}\int_{-\infty}^{\infty} x^{e,i}(\phi,\eta,t)g(\eta)d\eta. \tag{2.A.2}$$

Additionally, the quantity $y^{e,i}(\eta,t)$ is, for each value of η, the mean of the membrane potential $y^{e,i}(\phi,\eta,t) = \text{P.V.}\int_{-\infty}^{\infty}\rho^{e,i}(v^{e,i}|\eta,t,\phi)v^{e,i}\,dv^{e,i}$. Therefore, this variable is related to the mean membrane potential of the neuronal population at ϕ by

$$V^{e,i}(\phi,t) = \int_{-\infty}^{\infty} y^{e,i}(\phi,\eta,t)g(\eta)d\eta. \tag{2.A.3}$$

Substituting the LA (2.A.1) into the continuity equation, we find that, for each value of η, the variables $x^{e,i}(\phi)$ and $y^{e,i}(\phi)$ must obey two coupled equations which can be written in complex form as

$$\begin{aligned}\tau\partial_t w^{e,i}(\phi,\eta,t) = i\big[&\eta + \tau S(\phi,t) - \left(w^{e,i}\right)^2(\phi,\eta,t)\\ &+ P^{e,i}(\phi,t)\big],\end{aligned} \tag{2.A.4}$$

where $w^{e,i}(\phi,\eta,t) \equiv x^{e,i}(\phi,\eta,t) + iy^{e,i}(\phi,\eta,t)$. If η are distributed according to a Lorentzian distribution Eq. (2.5), the integrals in (2.A.2) and (2.A.3) can then be evaluated closing the integral contour in the complex η-plane, and using the Cauchy residue theorem. Then the firing rate and mean membrane potential depend only on the value of $w^{e,i}$ at the pole of $g(\eta)$ in the lower half η-plane: $\pi\tau R^{e,i}(\phi,t) + iV^{e,i}(\phi,t) = w^{e,i}(\phi,\bar{\eta}-i\Delta,t)$, and, as a result, (2.A.4)

must be evaluated only at $\eta = \bar{\eta} - i\Delta$ to obtain the neural field equations [Eq. (2.6)]*

These equations can be nondimensionalized by rescaling variables and time as (note the difference between $v_j^{e,i}$, the membrane potential of a single neuron j, and the mean membrane potential $v^{e,i}$):

$$R^{e,i} = \frac{\sqrt{\Delta}}{\tau} r^{e,i} \ , \ V^{e,i} = \sqrt{\Delta}\ v^{e,i} \ , \ t = \frac{\tau}{\sqrt{\Delta}} \tilde{t}, \tag{2.A.5}$$

and parameters as:

$$J_K^{e,i} = \sqrt{\Delta}\ j_K^{e,i},\ \bar{\eta} = \Delta\tilde{\eta},\ P^{e,i}(\phi, t) = \Delta \tilde{P}^{e,i}(\phi, \tilde{t}). \tag{2.A.6}$$

The resulting dimensionless NFM is then

$$\dot{r}^{e,i} = \frac{1}{\pi} + 2v^{e,i}r^{e,i}, \tag{2.A.7a}$$

$$\dot{v}^{e,i} = \left(v^{e,i}\right)^2 + \tilde{\eta} - \pi^2 \left(r^{e,i}\right)^2 + s(\phi, \tilde{t}) + \tilde{P}^{e,i}(\phi, \tilde{t}), \tag{2.A.7b}$$

where the overdot represents derivation with respect the nondimensional time $\tilde{t}$ and the mean field is

$$\begin{aligned} s(\phi, \tilde{t}) =& \frac{1}{\pi} \int_{-\pi}^{\pi} \left[\frac{j_0^e}{2} + \sum_{K=1}^{\infty} j_K^e \cos(K(\phi' - \phi)) \right] r^e(\phi', \tilde{t}) d\phi' \\ & - \frac{1}{\pi} \int_{-\pi}^{\pi} \left[\frac{j_0^i}{2} + \sum_{K=1}^{\infty} j_K^i \cos(K(\phi' - \phi)) \right] r^i(\phi', \tilde{t}) d\phi'. \end{aligned} \tag{2.A.8}$$

* The derivation of the QIF-NFM Eq. (2.6) can be readily extended to account for population of excitatory and inhibitory neurons of different sizes, i.e. $N^e \neq N^i$. This can be always achieved by rescaling the relative contributions of the excitatory and inhibitory mean fields as $S(\phi) = p^e S^e(\phi) + p^i S^i(\phi)$, where $p^e = 2N^e/\left(N^e + N^i\right)$ and $p^i = 2N^i/\left(N^e + N^i\right)$. In the case of the effective model Eq. (2.7), this implies that Fourier coefficients in Eq. (2.8) need to be changed as $J_K = p^e J_K^e - p^i J_K^i$.

2.A.1 Effective NFM model

Considering $\tilde{P}^{e,i}(\phi,\tilde{t}) = \tilde{P}(\phi,\tilde{t})$ in Eqs. (2.A.7), the system

$$\dot{r} = \frac{1}{\pi} + 2vr, \tag{2.A.9a}$$

$$\dot{v} = v^2 + \tilde{\eta} - \pi^2 r^2 + s(\phi,\tilde{t}) + \tilde{P}(\phi,\tilde{t}), \tag{2.A.9b}$$

with the mean field

$$s(\phi,t) = \frac{1}{\pi}\int_{-\pi}^{\pi}\left[\frac{j_0}{2} + \sum_{K=1}^{\infty} j_K \cos(K(\phi'-\phi))\right] r(\phi',t)d\phi'. \tag{2.A.10}$$

and

$$j_K = j_K^e - j_K^i,$$

has identical symmetric solutions as the original Eqs.(2.A.7), i.e.

$$r^e(t) = r^i(t) = r(t), \quad v^e(t) = v^i(t) = v(t).$$

2.B Linear stability analysis of the Spatially Homogeneous State

2.B.1 Linear stability of the effective QIF-NFM Eq. (2.7)

The homogeneous steady state is given by the solution of Eq. (2.9) when $R_*(\phi) = R_*$. This is equivalent to $S_*(\phi) = S_* = J_0 R_*$ that in dimensionless form is

$$\pi^2 r_*^4 - j_0 r_*^3 - \tilde{\eta} r_*^2 - \frac{1}{4\pi^2} = 0. \tag{2.B.1}$$

This equation is greatly simplified assuming $j_0 = 0$ and gives

$$r_* = \frac{1}{\pi\sqrt{2}}\sqrt{\tilde{\eta} + \sqrt{\tilde{\eta}^2 + 1}}. \tag{2.B.2}$$

The stability of homogeneous steady-state solutions can be analyzed studying the evolution of the small (even) perturbations ($\epsilon \ll 1$) of the SHS

$$r(\phi,t) = r_* + \epsilon \sum_{K=0}^{\infty} a_K(t)\cos(K\phi), \tag{2.B.3a}$$

$$v(\phi,t) = v_* + \epsilon \sum_{K=0}^{\infty} b_K(t)\cos(K\phi). \tag{2.B.3b}$$

Substituting (2.B.3) into the mean field (2.A.10), we obtain a perturbed mean field around $s_*(\phi)$

$$s(\phi,t) = s_*(\phi) + \epsilon \sum_{K=0}^{\infty} j_K a_K(t)\cos(K\phi). \tag{2.B.4}$$

Linearizing Eqs. (2.A.9) around the fixed point (r_*, v_*), gives

$$\sum_{K=0}^{\infty} \mu_K a_K \cos(K\phi) = 2\sum_{K=0}^{\infty} [r_*(\phi)b_K + v_*(\phi)a_K]\cos(K\phi), \tag{2.B.5}$$

$$\sum_{K=0}^{\infty} \mu_K b_K \cos(K\phi) = \sum_{K=0}^{\infty} \left[2v_*(\phi)b_K + (j_K - 2\pi^2 r_*(\phi))a_K\right]\cos(K\phi),$$

where we have used the ansatz $a_K(t) = a_K e^{\mu_K t}$ and $b_K(t) = b_K e^{\mu_K t}$, where μ_K represents the dimensionless eigenvalue of the Kth mode. For SHS states, $(r_*(\phi), v_*(\phi)) = (r_*, v_*)$, the modes in Eqs. (2.B.6) decouple and, for a given mode K, we find the linear system

$$\mu_K \begin{pmatrix} a_K \\ b_K \end{pmatrix} = L_* \begin{pmatrix} a_K \\ b_K \end{pmatrix}, \tag{2.B.6}$$

with:

$$L_* = \begin{pmatrix} 2v_* & 2r_* \\ j_K - 2\pi^2 r_* & 2v_* \end{pmatrix}. \tag{2.B.7}$$

Equation (2.B.6) has a general solution:

$$\begin{pmatrix} a_K(\tilde{t}) \\ b_K(\tilde{t}) \end{pmatrix} = A_+ \mathbf{u}_+ e^{\mu_{K+}\tilde{t}} + A_- \mathbf{u}_- e^{\mu_{K-}\tilde{t}}, \tag{2.B.8}$$

where $A_\pm$ are arbitrary constants. The eigenvalues $\mu_{K\pm}$ are given by

$$\mu_{K\pm} = -\frac{1}{\pi r_*} \pm 2\pi r_* \sqrt{\frac{j_K}{2\pi^2 r_*} - 1}, \tag{2.B.9}$$

with eigenvectors

$$\mathbf{u}_\pm = \begin{pmatrix} \pm 1 \\ \sqrt{\frac{j_K}{2r_*} - \pi^2} \end{pmatrix}. \tag{2.B.10}$$

In terms of the dimensional variables and parameters (2.A.5) and (2.A.6), the eigenvalues (2.B.9) are $\lambda_k t = \mu_k \tilde{t}$, and thus $\lambda_k = \sqrt{\Delta}\mu_k/\tau$, which gives the eigenvalues Eq. (2.10) in the main text.

2.B.2 Linear stability of the full QIF-NFM

For the full QIF-NFM Eq. (2.6), the perturbation around the SHS state has the form

$$\begin{aligned} r^{e,i}(\phi,t) &= r_* + \epsilon \sum_{K=0}^{\infty} a_K^{e,i}(t)\cos(K\phi), \\ v^{e,i}(\phi,t) &= v_* + \epsilon \sum_{K=0}^{\infty} b_K^{e,i}(t)\cos(K\phi). \end{aligned}$$

In this case, the linear stability of the SHS state with respect to perturbations of the K-spatial mode is determined by the characteristic equation

$$\lambda_K \begin{pmatrix} a_K^e \\ b_K^e \\ a_K^i \\ b_K^i \end{pmatrix} = \begin{pmatrix} 2v_* & 2r_* & 0 & 0 \\ j_K^e - 2\pi^2 r_* & 2v_* & -j_K^i & 0 \\ 0 & 0 & 2v_* & 2r_* \\ j_K^e & 0 & -j_K^i - 2\pi^2 r_* & 2v_* \end{pmatrix} \begin{pmatrix} a_K^e \\ b_K^e \\ a_K^i \\ b_K^i \end{pmatrix} \tag{2.B.11}$$

For each K mode, the linearized system has a general solution

$$\begin{aligned} \begin{pmatrix} a_K^e(\tilde{t}) \\ b_K^e(\tilde{t}) \\ a_K^i(\tilde{t}) \\ b_K^i(\tilde{t}) \end{pmatrix} = \; & A_+ \quad \mathbf{u}_{K+} e^{\mu_{K+}\tilde{t}} + A_- \mathbf{u}_{K-} e^{\mu_{K-}\tilde{t}} + \\ & B_+ \quad \mathbf{u}_{K\perp} e^{\mu_\perp \tilde{t}} + B_- \bar{\mathbf{u}}_{K\perp} e^{\bar{\mu}_\perp \tilde{t}}, \end{aligned} \tag{2.B.12}$$

where $A_\pm$ and $B_\pm$ are arbitrary constants. The eigenvectors

$$\mathbf{u}_{K\pm} = \begin{pmatrix} \pm 1 \\ \sqrt{\frac{j_K^e - j_K^i}{2r_*} - \pi^2} \\ \pm 1 \\ \sqrt{\frac{j_K^e - j_K^i}{2r_*} - \pi^2} \end{pmatrix}. \tag{2.B.13}$$

have eigenvalues

$$\mu_{K\pm} = -\frac{1}{\pi r_*} \pm 2\pi r_* \sqrt{\frac{j_K^e - j_K^i}{2\pi^2 r_*} - 1}. \tag{2.B.14}$$

These eigenvalues coincide with those of the reduced system (2.B.9), and are associated with the standing waves shown in Fig. 2.2. Additionally, the eigenvector

$$\mathbf{u}_{K\perp} = \begin{pmatrix} i j_K^i \\ \pi j_K^i \\ i j_K^e \\ \pi j_K^e \end{pmatrix}, \tag{2.B.15}$$

and its complex conjugate $\bar{\mathbf{u}}_{K\perp}$, with the associated eigenvalue

$$\mu_\perp = -\frac{1}{\pi r_*} + i 2\pi r_*, \tag{2.B.16}$$

and its complex conjugate $\bar{\mu}_\perp$, correspond to modes of oscillation of the uncoupled system. Indeed, note that the eigenvalues (2.B.16) are independent of the connectivity, and correspond to oscillatory modes which are already present in a single population of uncoupled neurons —note that eigenvalues (2.B.14) reduce to (2.B.16) for all the modes with $j_K = j_K^e - j_K^e = 0$.

2.C Small-amplitude equation near the Spatially Homogeneous State

2.C.1 Critical eigenvectors

Right at the bifurcation, the only undamped mode is the critical one given by $\mathbf{u}_+$ in (2.B.10), that reduces to the critical eigenmode:

$$\mathbf{u}_c = \begin{pmatrix} r_* \\ -v_* \end{pmatrix}. \tag{2.C.1}$$

At criticality, the critical eigenmode of L_* satisfies

$$L_{*c}\mathbf{u}_c = 0,$$

where L_{*c} corresponds to the operator (2.B.7) evaluated at $j_K = j_{Kc}$. The left critical eigenvector of the operator L_{*c} is then defined as

$$\mathbf{u}_c^\dagger L_{*c} = 0,$$

which gives

$$\mathbf{u}_c^\dagger = \pi \begin{pmatrix} -v_* \\ r_* \end{pmatrix}^T, \tag{2.C.2}$$

where the constant has been taken to normalize the eigenvectors, so that they satisfy $\mathbf{u}_c^\dagger \mathbf{u}_c = 1$.

2.C.2 Amplitude equation

Except for initial transients, the amplitude of the bifurcating solution at criticality is expected to contain only the component $\mathbf{u}_{+c}$. In the following we derive a small-amplitude equation for the bump solutions using multiple-scale analysis, (Kuramoto, 1984, see e.g.). First, let the solution of Eqs. (2.A.9) be written as the perturbation expansion

$$\begin{pmatrix} r(\phi,\tilde{t}) \\ v(\phi,\tilde{t}) \end{pmatrix} = \begin{pmatrix} r_* \\ v_* \end{pmatrix} + \epsilon \begin{pmatrix} r_\epsilon(\phi,\tilde{t},\tilde{T}) \\ v_\epsilon(\phi,\tilde{t},\tilde{T}) \end{pmatrix} + \epsilon^2 \begin{pmatrix} r_{\epsilon\epsilon}(\phi,\tilde{t},\tilde{T}) \\ v_{\epsilon\epsilon}(\phi,\tilde{t},\tilde{T}) \end{pmatrix} + \dots \tag{2.C.3}$$

where (r_*, v_*) is the state SHS given by the solutions of (2.B.1), and $\epsilon \ll 0$ is a small parameter, which measures the distance from the Turing bifurcation. In addition, we define a long time scale, $\tilde{T} = \epsilon^2 \tilde{t}$, that is considered to be independent of $\tilde{t}$. Accordingly, the differential operator in Eqs. (2.A.9) may be replaced by:

$$\partial_{\tilde{t}} \to \partial_{\tilde{t}} + \epsilon^2 \partial_{\tilde{T}}.$$

Since the asymptotic expansion is going to be performed in the vicinity of a stationary bifurcation, we set $\partial_{\tilde{t}} = 0$ so that the only temporal variations occur with the slow time scale $\tilde{T}$.

Additionally, in our analysis we use the parameter j_1 as the bifurcation parameter, and we write it as

$$j_1 = j_1^T + \epsilon^2 \delta j_1, \tag{2.C.4}$$

where j_1^T is the critical value of j_1 at which the Turing bifurcation occurs, given by Eq. (2.11), with $K = 1$. Accordingly, the (nondimensionalized) connectivity footprint (2.1) is

$$j(\phi) = j_c(\phi) + 2\epsilon^2 \delta j_1 \cos\phi, \tag{2.C.5}$$

with

$$j_c(\phi) = j_0 + 2j_1^T \cos\phi + 2\sum_{K=2}^{\infty} j_K \cos(K\phi), \tag{2.C.6}$$

where $j_K < j_{Kc}$ for $K \neq 1$. To simplify the notation, we hereafter omit to explicitly write the dependence of $r_{\epsilon,\epsilon\epsilon,\dots}$ and $v_{\epsilon,\epsilon\epsilon,\dots}$ on the variables $\tilde{t}, T$ and ϕ. Substituting (2.C.3) and (2.C.5) into the mean field (2.A.10):

$$\begin{aligned}
s(\phi) &= \frac{1}{2\pi}\int_{-\pi}^{\pi} (r_* + \epsilon r_\epsilon + \epsilon^2 r_{\epsilon\epsilon} + \dots) j_c(\phi - \phi') d\phi' \\
&\quad + \epsilon^2 \frac{1}{\pi}\int_{-\pi}^{\pi} (r_* + \epsilon r_\epsilon + \epsilon^2 r_{\epsilon\epsilon} + \dots)\ \delta j_1 \cos(\phi - \phi') d\phi' \\
&\equiv \langle r_* + \epsilon r_\epsilon + \epsilon^2 r_{\epsilon\epsilon} + \dots \rangle_c \\
&\quad + 2\epsilon^2 \langle r_* + \epsilon r_\epsilon + \epsilon^2 r_{\epsilon\epsilon} + \dots \rangle \qquad (2.C.7) \\
&= r_* j_0 + \epsilon \langle r_\epsilon \rangle_c + \epsilon^2 \langle r_{\epsilon\epsilon} \rangle_c + \epsilon^3 (\langle r_{\epsilon\epsilon\epsilon} \rangle_c + 2\langle r_\epsilon \rangle) + \dots \qquad (2.C.8)
\end{aligned}$$

Plugging expansions (2.C.3) and (2.C.5) into the NFM Eqs. (2.A.9), we obtain

$$\begin{aligned}
\epsilon^2\partial_{\tilde{T}}(\epsilon r_\epsilon + \epsilon^2 r_{\epsilon\epsilon} + \dots) &= \epsilon(2v_* r_\epsilon + 2r_* v_\epsilon) \\
&\quad +\epsilon^2(2v_* r_{\epsilon\epsilon} + 2r_\epsilon v_\epsilon + 2r_* v_{\epsilon\epsilon}) \\
&\quad +\epsilon^3(2v_\epsilon r_{\epsilon\epsilon} + 2r_\epsilon v_{\epsilon\epsilon}) + \dots \\
\epsilon^2\partial_{\tilde{T}}(\epsilon v_\epsilon + \epsilon^2 v_{\epsilon\epsilon} + \dots) &= \epsilon(2v_* v_\epsilon - 2\pi^2 r_* r_\epsilon + \langle r_\epsilon\rangle_c) \\
&\quad +\epsilon^2(v_\epsilon^2 - \pi^2 r_\epsilon^2 + 2v_* v_{\epsilon\epsilon} - 2\pi^2 r_* r_{\epsilon\epsilon} + \langle r_{\epsilon\epsilon}\rangle_c) \\
&\quad +\epsilon^3(2v_\epsilon v_{\epsilon\epsilon} - 2\pi^2 r_\epsilon r_{\epsilon\epsilon} + \langle r_{\epsilon\epsilon\epsilon}\rangle_c + 2\langle r_\epsilon\rangle) + \dots
\end{aligned}$$

These equations can be written in a more compact form as

$$-(L_c+\epsilon^2 L_{\epsilon\epsilon})\left[\epsilon\begin{pmatrix} r_\epsilon \\ v_\epsilon\end{pmatrix} + \epsilon^2\begin{pmatrix} r_{\epsilon\epsilon} \\ v_{\epsilon\epsilon}\end{pmatrix} + ...\right] = \epsilon^2 N_{\epsilon\epsilon}+\epsilon^3 N_{\epsilon\epsilon\epsilon}+\dots, \quad (2.C.9)$$

defining the linear and nonlinear operators

$$\begin{aligned}
L_c &= \begin{pmatrix} 2v_* & 2r_* \\ \langle\cdot\rangle_c - 2\pi^2 r_* & 2v_*\end{pmatrix}, \\
L_{\epsilon\epsilon} &= \begin{pmatrix} -\partial_{\tilde{T}} & 0 \\ 2\langle\cdot\rangle & -\partial_{\tilde{T}}\end{pmatrix}, \\
N_{\epsilon\epsilon} &= \begin{pmatrix} 2r_\epsilon v_\epsilon \\ v_\epsilon^2 - \pi^2 r_\epsilon^2\end{pmatrix}, \\
N_{\epsilon\epsilon\epsilon} &= \begin{pmatrix} 2r_\epsilon v_{\epsilon\epsilon} + 2r_{\epsilon\epsilon} v_\epsilon \\ 2v_\epsilon v_{\epsilon\epsilon} - 2\pi^2 r_\epsilon r_{\epsilon\epsilon}\end{pmatrix},
\end{aligned}$$

Next we collect terms by order in ϵ. At first order we recover the linear problem (2.B.6) at the Turing bifurcation:

$$\begin{pmatrix} 2v_* & 2r_* \\ j_1^T - 2\pi^2 r_* & 2v_*\end{pmatrix}\begin{pmatrix} r_\epsilon \\ v_\epsilon\end{pmatrix} = \begin{pmatrix} 0 \\ 0\end{pmatrix}.$$

Recalling that j_1^T is given by Eq. (2.C.4), we find the neutral solution:

$$\begin{pmatrix} r_\epsilon \\ v_\epsilon\end{pmatrix} = A\ \mathbf{u}_c \cos\phi, \quad (2.C.10)$$

where A is the small amplitude with slow time dependence that we aim to determine and $\mathbf{u}_c$ is the critical eigenmode given by Eq. (2.C.1). Substituting the solution (2.C.10) into the nonlinear forcing terms $N_{\epsilon\epsilon}$ we find

$$N_{\epsilon\epsilon} = \frac{A^2}{2}\begin{pmatrix} \pi^{-1} \\ v_*^2 - \pi^2 r_*^2 \end{pmatrix}[1 + \cos(2\phi)],$$

what implies that, at second order, the solution must necessarily contain homogeneous and second spatial components

$$\begin{pmatrix} r_{\epsilon\epsilon} \\ v_{\epsilon\epsilon} \end{pmatrix} = \begin{pmatrix} r_{\epsilon\epsilon 0} \\ v_{\epsilon\epsilon 0} \end{pmatrix} + \begin{pmatrix} r_{\epsilon\epsilon 2} \\ v_{\epsilon\epsilon 2} \end{pmatrix} \cos(2\phi).$$

Equating the homogeneous, second order terms of equation (2.C.9) we find

$$-\begin{pmatrix} 2v_* & 2r_* \\ j_0 - 2\pi^2 r_* & 2v_* \end{pmatrix}\begin{pmatrix} r_{\epsilon\epsilon 0} \\ v_{\epsilon\epsilon 0} \end{pmatrix} = \frac{A^2}{2}\begin{pmatrix} \pi^{-1} \\ v_*^2 - \pi^2 r_*^2 \end{pmatrix},$$

and left-multiplying this equation by L_c^{-1}, and using Eq. (2.12) we find

$$\begin{pmatrix} r_{\epsilon\epsilon 0} \\ v_{\epsilon\epsilon 0} \end{pmatrix} = \frac{A^2}{4r_*(j_1^T - j_0)}\begin{pmatrix} 2v_* & -2r_* \\ 2\pi^2 r_* - j_0 & 2v_* \end{pmatrix}\begin{pmatrix} \pi^{-1} \\ v_*^2 - \pi^2 r_*^2 \end{pmatrix},$$

which gives the coefficients

$$r_{\epsilon\epsilon 0} = \frac{3v_*^2 - \pi^2 r_*^2}{2(j_1^T - j_0)}A^2, \tag{2.C.11}$$

$$v_{\epsilon\epsilon 0} = \frac{2\pi v_*^4 - v_* j_0 - 3\pi/2}{2(j_1^T - j_0)}A^2. \tag{2.C.12}$$

Proceeding similarly, we find the coefficients corresponding to the second spatial Fourier modes:

$$r_{\epsilon\epsilon 2} = \frac{3v_*^2 - \pi^2 r_*^2}{2(j_1^T - j_2)}A^2, \tag{2.C.13}$$

$$v_{\epsilon\epsilon 2} = \frac{2\pi v_*^4 - v_* j_2 - 3\pi/2}{2(j_1^T - j_2)}A^2. \tag{2.C.14}$$

Collecting the third-order terms of equation (2.C.9), we obtain the identity

$$-L_c\begin{pmatrix} r_{\epsilon\epsilon\epsilon} \\ v_{\epsilon\epsilon\epsilon}\end{pmatrix} - L_{\epsilon\epsilon}\begin{pmatrix} r_{\epsilon} \\ v_{\epsilon}\end{pmatrix} = N_{\epsilon\epsilon\epsilon}. \tag{2.C.15}$$

To obtain the desired amplitude equation, we shall left-multiply Eq. (2.C.15) by the left null-eigenvector (2.C.2) and project it into the first spatial Fourier mode. The first term on the right-hand side of Eq. (2.C.15) vanishes since $\mathbf{u}_c^\dagger L_c = 0$. The second term is

$$L_{\epsilon\epsilon}\begin{pmatrix} r_{\epsilon} \\ v_{\epsilon}\end{pmatrix} = \begin{pmatrix} -r_* \ \partial_{\tilde{T}} A \\ v_* \ \partial_{\tilde{T}} A + \delta j_1 \ r_* \ A\end{pmatrix} \cos\phi.$$

Finally, the nonlinear forcing term at the left-hand side of Eq. (2.C.15) is

$$\begin{aligned} N_{\epsilon\epsilon\epsilon} \ &= \ -A\cos\phi\begin{pmatrix} v_*\alpha - r_*\beta \\ \pi^2 r_*\alpha + v_*\beta\end{pmatrix} \\ &\quad -A\cos(3\phi)\begin{pmatrix} v_* r_{\epsilon\epsilon 2} - r_* v_{\epsilon\epsilon 2} \\ \pi^2 r_* r_{\epsilon\epsilon 2} + v_* v_{\epsilon\epsilon 2}\end{pmatrix}, \end{aligned}$$

where $\alpha = (2r_{\epsilon\epsilon 0} + r_{\epsilon\epsilon 2})$ and $\beta = (2v_{\epsilon\epsilon 0} + v_{\epsilon\epsilon 2})$. Thus, the solvability condition gives

$$\mathbf{u}_c^\dagger\begin{pmatrix} r_* \ \partial_{\tilde{T}} A \\ -v_* \ \partial_{\tilde{T}} A - \delta j_1 \ r_* \ A\end{pmatrix} = -A\mathbf{u}_c^\dagger\begin{pmatrix} v_*\alpha - r_*\beta \\ \pi^2 r_*\alpha + v_*\beta\end{pmatrix}. \tag{2.C.16}$$

Substituting the coefficients (2.C.11), (2.C.12), (2.C.13), and (2.C.14) into Eq. (2.C.16) gives the desired amplitude equation

$$\partial_{\tilde{T}} A = \pi r_*^2 \ \delta j_1 A + \tilde{a} A^3, \tag{2.C.17}$$

where the parameter $\tilde{a}$ is

$$\begin{aligned} \tilde{a} =& \pi\left(5v_*^4 + \pi^4 r_*^4 - \frac{5}{2}\right)\left(\frac{1}{j_1^T - j_0} + \frac{1/2}{j_1^T - j_2}\right) \\ & - v_*\left(\frac{j_0}{j_1^T - j_0} + \frac{j_2/2}{j_1^T - j_2}\right). \end{aligned} \tag{2.C.18}$$

Equating Eq. (2.C.18) to zero, gives the critical boundary j_2^c separating subcritical and supercritical Turing bifurcations:

$$j_2^c = \frac{3j_1^T - j_0}{2} + \frac{6(j_1^T - j_0)^2\pi^2 r_*^3}{5 + 4\pi^2 r_*^3(3j_0 - j_1^T - 10\pi^2 r_* + 4\pi^6 r_*^5)}. \quad (2.C.19)$$

In dimensional form, Eqs. (2.C.17), (2.C.18), and (2.C.19) are respectively:

$$\tau\partial_T A = \pi\frac{\tau^2 R_*^2}{\Delta}\,\delta J_1 A + aA^3, \quad (2.C.20)$$

$$a = \left[\pi\left(\frac{5\Delta^3}{16\pi^4\tau^4 R_*^4} + \frac{\pi^4\tau^4 R_*^4}{\Delta} - \frac{5\Delta}{2}\right)\left(\frac{1}{J_1^T - J_0} + \frac{1/2}{J_1^T - J_2}\right) + \frac{\Delta}{2\pi\tau R_*}\left(\frac{J_0}{J_1^T - J_0} + \frac{J_2/2}{J_1^T - J_2}\right)\right], \quad (2.C.21)$$

and

$$J_2^c = \frac{3J_1^T - J_0}{2} + \frac{6(J_1^T - J_0)^2\pi^2\tau^3 R_*^3}{5\Delta^2 + 4\pi^2\tau^3 R_*^3\left(3J_0 - J_1^T - 10\pi^2\tau R_* + \frac{4\pi^6\tau^5 R_*^5}{\Delta^2}\right)}. \quad (2.C.22)$$

2.D Numerical simulations

2.D.1 Numerical simulation of the QIF model

In numerical simulations we used the Euler scheme with time step $dt = 10^{-3}$. Additionally, we considered the peak and reset values $v_p = -v_r = 100$. The algorithm used to simulate the QIF neuron (2.2) is shown in Fig. 2.D.1.

2.D.2 Numerical simulation of the ring network

To numerically implement the ring network of QIF neurons we divided the ring into $m = 100$ intervals located at $\phi_l = 2\pi l/m - \pi$, $l =$

Require: Variables: v_j, I_j, t_j^r (exit time from refractory period), t (time). Constants: τ, dt, v_p.
Ensure: $\dot{v}_j = v_j^2 + I_j$ and t_j^l and t_j^r.

bool spike$_j$ $\leftarrow$ **False**
if $t \geq t_j^r$ **then** ▷ Check whether the neuron is in the refractory period.
    $v_j \leftarrow v_j + \frac{dt}{\tau}\left(v_j^2 + I_j\right)$ ▷ Euler integration.
    if $v_j \geq v_p$ **then** ▷ Check if the voltage has crossed the threshold.
        spike$_j$ $\leftarrow$ **True** ▷ The neuron has spiked at time t_j^l.
        $t_j^r \leftarrow t + 2 \cdot \frac{\tau}{v_j}$ ▷ Set the end of the refractory period.
        $t_j^l \leftarrow t + \frac{\tau}{v_j}$ ▷ Spike time is set after $\frac{\tau}{v_j}$.
        $v_j \leftarrow -v_j$ ▷ Reset the voltage.
    end if
end if

Figure 2.D.1: Algorithm used for the Euler integration of the QIF neuron Eq. (2.2).

$1, \ldots, m$. At each interval ϕ_l, we considered $n = 2.5 \cdot 10^3$ excitatory and $n = 2.5 \cdot 10^3$ inhibitory neurons (i.e. the ring consisted of a total of $2N = 2m$ $n = 5 \times 10^5$ QIF neurons).

The neurons in each location ϕ_l receive Lorentzian-distributed currents, which have been generated using the formula

$$\eta_i = \bar{\eta} + \Delta \tan\left[\frac{\pi}{2}\frac{2i - n - 1}{n + 1}\right], \; i = 1, \ldots, n. \tag{2.D.1}$$

On the other hand, perturbations (applied at time t_0) are modeled using the function

$$P^{e,i}(\phi, t) = A\left(e^{(t-t_0)/\tau_r} - 1\right) \cdot \cos\left(K \cdot \phi\right), \tag{2.D.2}$$

where A is the amplitude, K is the wave number, and τ_r is the rising time constant of the perturbation. In Figs. 2.2, 2.3 and 2.5 we used $t_0 = 0.05$ s, $A = 0.3$, and $\tau_r = 4 \times 10^{-3}$ s. The perturbations had a duration of $\Delta t = 0.01$ s.

Finally, the instantaneous firing rates in Fig. 2.2 are obtained binning time and counting the spikes of neurons in each interval ϕ_l within a sliding time window of size $\delta t = 0.01$s.

CHAPTER 3

Synchrony-induced persistent oscillations in a E-I neural network

This work is being developed in collaboration with David Fernández-Boshman, and Ernest Montbrió.

"Quote"

— Author, Title of Source.

Conclusions

hola

APPENDIX A

Generalization of the QIF-FR model

APPENDIX B

Numerical simulations of QIF neural networks

Methodology used for numerical integration of the differential equations, measurements, etc. Links to the code and algorithms.

References

Abbott, L. F. (1999). Lapicque's introduction of the integrate-and-fire model neuron (1907). *Brain Research Bulletin*, 50(5-6):303–304.

Abbott, L. F. and Van Vreeswijk, C. (1993). Asynchronous states in networks of pulse-coupled oscillators. *Physical Review E*, 48(2):1483–1490.

Amari, S.-I. (1972). Characteristics of Random Nets of Analog Neuron-Like Elements. *IEEE Transactions on Systems, Man and Cybernetics*, 2(5):643–657.

Amari, S.-I. (1974). A method of statistical neurodynamics. *Kybernetik*, 14(4):201–215.

Amari, S.-I. (1977). Dynamics of pattern formation in lateral-inhibition type neural fields. *Biological cybernetics*, 87:77–87.

Andersen, P. and Eccles, J. (1962). Inhibitory Phasing of Neuronal Discharge. *Nature*, 196(4855):645–647.

Atay, F. M. and Hutt, A. (2004). Stability and Bifurcations in Neural Fields with Finite Propagation Speed and General Connectivity. *SIAM Journal on Applied Mathematics*, 65(2):644–666.

Avitabile, D. (2016). Numerical computation of coherent structures in spatially-extended systems. *Second International Conference on Mathematical Neuroscience, Antibes Juan-les-Pins*.

Avitabile, D., Desroches, M., and Knobloch, E. (2017). Spatiotemporal canards in neural field equations. *Physical Review E*, 95(4):1–8.

Bartos, M., Vida, I., and Jonas, P. (2007). Synaptic mechanisms of synchronized gamma oscillations in inhibitory interneuron networks. *Nature Reviews Neuroscience*, 8(1):45–56.

Battaglia, D., Brunel, N., and Hansel, D. (2007). Temporal Decorrelation of Collective Oscillations in Neural Networks with Local Inhibition and Long-Range Excitation. *Phys. Rev. Lett.*, 99(23):238106.

Berger, H. (1929). Über das Elektrenkephalogramm des Menschen. *Archiv für Psychiatrie und Nervenkrankheiten*, 87(1):527–570.

Beurle, R. L. (1956). Properties of a mass of cells capable of regenerating pulses. *Philosophical Transactions of the Royal Society of London. Series B, Biological Sciences*, 240(669):55–94.

Bressloff, P. C. (2012). Spatiotemporal dynamics of continuum neural fields. *Journal of Physics A: Mathematical and Theoretical*, 45(3):033001.

Brunel, N. (2000). Dynamics of networks of randomly connected excitatory and inhibitory spiking neurons. *Journal of Physiology-Paris*, 94(5-6):445–463.

Brunel, N., Chance, F. S., Fourcaud, N., and Abbott, L. F. (2001). Effects of synaptic noise and filtering on the frequency response of spiking neurons. *Physical Review Letters*, 86(10):2186–2189.

Brunel, N. and Hakim, V. (1999). Fast global oscillations in networks of integrate-and-fire neurons with low firing rates. *Neural computation*, 11(7):1621–1671.

Brunel, N. and Hansel, D. (2006). How noise affects the synchronization properties of recurrent networks of inhibitory neurons. *Neural Comput.*, 18(5):1066–1110.

Brunel, N. and Van Rossum, M. C. (2007a). Lapicque's 1907 paper: From frogs to integrate-and-fire. *Biological Cybernetics*, 97(5-6):337–339.

Brunel, N. and Van Rossum, M. C. (2007b). Quantitative investigations of electrical nerve excitation treated as polarization. *Biological Cybernetics*, 97(5-6):341–349.

Brunel, N. and Wang, X.-J. (2003). What determines the frequency of fast network oscillations with irregular neural discharges? I. Synaptic dynamics and excitation-inhibition balance. *Journal of neurophysiology*, 90(1):415–430.

Buzsaki, G. (2004). Neuronal Oscillations in Cortical Networks. *Science*, 304(5679):1926–1929.

Buzsaki, G. (2006). *Rhythms of the Brain*. Oxford University Press.

Buzsáki, G. and Moser, E. I. (2013). Memory, navigation and theta rhythm in the hippocampal-entorhinal system. *Nature Neuroscience*, 16(2):130–138.

Byrne, Á., Brookes, M. J., and Coombes, S. (2017). A mean field model for movement induced changes in the beta rhythm. *Journal of Computational Neuroscience*, 43(2):143–158.

Chandra, S., Hathcock, D., Crain, K., Antonsen, T. M., Girvan, M., and Ott, E. (2017). Modeling the network dynamics of pulse-coupled neurons. *Chaos*, 27(3).

Coombes, S. (2005). Waves, bumps, and patterns in neural field theories. *Biological Cybernetics*, 93(2):91–108.

Coombes, S., beim Graben, P., and Potthast, R. (2014). Tutorial on neural field theory. In *Neural fields*, pages 1–43. Springer.

Coombes, S. and Byrne, Á. (2019). Next generation neural mass models. In *Lecture Notes in Nonlinear Dynamics in Computational Neuroscience: from Physics and Biology to ICT*. Springer. In press.

Coombes, S. and Laing, C. (2009). Delays in activity-based neural networks. *Philosophical transactions. Series A, Mathematical, physical, and engineering sciences*, 367(1891):1117–29.

Coombes, S., Lord, G. J., and Owen, M. R. (2003). Waves and bumps in neuronal networks with axo-dendritic synaptic interactions. *Physica D: Nonlinear Phenomena*, 178(3-4):219–241.

Cragg, B. and Temperley, H. (1954). The organisation of neurones: A co-operative analogy. *Electroencephalography and Clinical Neurophysiology*, 6(1952):85–92.

Deco, G., Jirsa, V. K., Robinson, P. a., Breakspear, M., and Friston, K. (2008). The dynamic brain: from spiking neurons to neural masses and cortical fields. *PLoS computational biology*, 4(8):e1000092.

Destexhe, A. and Sejnowski, T. J. (2009). The Wilson-Cowan model, 36 years later. *Biological Cybernetics*, 101(1):1–2.

Devalle, F., Roxin, A., and Montbrió, E. (2017). Firing rate equations require a spike synchrony mechanism to correctly describe fast oscillations in inhibitory networks. *PLoS Computational Biology*, 13(12):1–21.

Dijkstra, K., Gils, S. A. V., Janssens, S. G., Kuznetsov, Y. A., and Visser, S. (2015). Pitchfork-Hopf bifurcations in 1D neural field models with transmission delays. *Physica D: Nonlinear Phenomena*, 297:88–101.

Ermentrout, B. (1994). Reduction of Conductance-Based Models with Slow Synapses to Neural Nets. *Neural Computation*, 6(4):679–695.

Ermentrout, B. (1998). Neural networks as spatio-temporal pattern-forming systems. *Rep. Prog. Phys.*, 61(4):353.

Ermentrout, G. B. (1996). Type I neurons, phase resettings curves and synchrony. *Neural Comput*, 8(5):979–1001.

Ermentrout, G. B. and Kopell, N. (1986). Parabolic Bursting in an Excitable System Coupled with a Slow Oscillation.

Ermentrout, G. B. and Terman, D. H. (2010). *Mathematical foundations of neuroscience*, volume 64. Springer.

Esnaola-Acebes, J. M., Roxin, A., Avitabile, D., and Montbrió, E. (2017). Synchrony-induced modes of oscillation of a neural field model. *Physical Review E*, 96(5):052407.

Fourcaud, N. and Brunel, N. (2002). Dynamics of the Firing Probability of Noisy Integrate-and-Fire Neurons. *Neural Computation*, 14(9):2057–2110.

Fourcaud-Trocmé, N., Hansel, D., van Vreeswijk, C., and Brunel, N. (2003). How spike generation mechanisms determine the neuronal response to fluctuating inputs. *J. Neurosci.*, 23(37):11628–11640.

Freeman, W. J. (1964). A linear distributed feedback model for prepyriform cortex. *Experimental Neurology*, 10(6):525–547.

Freeman, W. J. (1967). Analysis of Function of Cerebral Cortex by use of Control Systems Theory. *The Logistics Rev*, 3:5–40.

Freeman, W. J. (1968a). Analog simulation of prepyriform cortex in the cat. *Mathematical Biosciences*, 2(1-2):181–190.

Freeman, W. J. (1968b). Relations between unit activity and evoked potentials in prepyriform cortex of cats. *Journal of Neurophysiology*, 31(3):337–348.

Freeman, W. J. (1975). *Mass action in the nervous system : examination of the neurophysiological : examination of the neurophysiological basis of adaptive behavior trough the EEG.* Academic Press, New York.

Fusi, S. and Mattia, M. (1999). Collective Behavior of Networks with Linear (VLSI) Integrate-and-Fire Neurons. *Neural Computation*, 11(3):633–652.

Gallego, R., Montbrió, E., and Pazó, D. (2017). Synchronization scenarios in the Winfree model of coupled oscillators. *Physical Review E*, 96(4):1–11.

Geisler, C. D. and Goldberg, J. M. (1966). A Stochastic Model of the Repetitive Activity of Neurons. *Biophysical Journal*, 6(1):53–69.

Gerstner, W. (2000). Population dynamics of spiking neurons: fast transients, asynchronous states, and locking. *Neural Comput.*, 12(1):43–89.

Gerstner, W., Kistler, W. M., Naud, R., and Paninski, L. (2014). *Neuronal dynamics : from single neurons to networks and models of cognition.* Cambridge University Press, Cambridge, United Kingdom.

Gloveli, T., Kopell, N., and Dugladze, T. (2010). Neuronal Activity Patterns During Hippocampal Network Oscillations In Vitro. In Cutsuridis, V., Graham, B., Cobb, S., and Vida, I., editors, *Hippocampal Microcircuits*, pages 247–276. Springer New York, New York, NY.

Griffith, J. S. (1963). On the stability of brain-like structures. *Biophysical journal*, 3:299–308.

Grossberg, S. (1973). Contour Enhancement, Short Term Memory, and Constancies in Reverberating Neural Networks. *Studies in Applied Mathematics*, 52(3):213–257.

Hansel, D. and Mato, G. (2001). Existence and stability of persistent states in large neuronal networks. *Physical Review Letters*, 86(18):4175–4178.

Hansel, D. and Mato, G. (2003). Asynchronous States and the Emergence of Synchrony in Large Networks of Interacting Excitatory and Inhibitory Neurons. *Neural Computation*, 15(1):1–56.

Hill, A. V. (1936). Excitation and accommodation in nerve. *Proceedings of the Royal Society of London. Series B, Biological Sciences*, 119(814):305–355.

Hodgkin, A. and Huxley, A. (1952). A quantitative description of membrane current and its application to conduction and excitation in nerve. *The Journal of physiology*, pages 500–544.

Hubel, D. H. and Wiesel, T. N. (1962). Receptive fields, binocular interaction and functional architecture in the cat's visual cortex. *The Journal of Physiology*, 160(1):106–154.

Hubel, D. H. and Wiesel, T. N. (1968). Receptive fields and functional architecture of monkey striate cortex. *The Journal of physiology*, 195(1):215–43.

Hutt, A. (2008). Local excitation-lateral inhibition interaction yields oscillatory instabilities in nonlocally interacting systems involving finite propagation delay. *Physics Letters, Section A: General, Atomic and Solid State Physics*, 372(5):541–546.

Izhikevich, E. M. (2007). *Dynamical Systems in Neuroscience: The Geometry of Excitability and Burtsing*. The MIT Press, Cambridge, Massachusetts.

Jansen, B. H. and Rit, V. G. (1995). Electroencephalogram and visual evoked potential generation in a mathematical model of coupled cortical columns. *Biological Cybernetics*, 73(4):357–366.

Jansen, B. H., Zouridakis, G., and Brandt, M. E. (1993). A neurophysiologically-based mathematical model of flash visual evoked potentials. *Biological Cybernetics*, 68(3):275–283.

Jirsa, V. and Haken, H. (1997). A derivation of a macroscopic field theory of the brain from the quasi-microscopic neural dynamics. *Physica D: Nonlinear Phenomena*, 99(4):503–526.

Kawamura, Y. (2014). From the Kuramoto-Sakaguchi model to the Kuramoto-Sivashinsky equation. *Physical Review E*, 2(11):1–6.

Knight, B. W. (1972). Dynamics of encoding in a population of neurons. *The Journal of general physiology*, 59(6):734–766.

Knight, B. W., Omurtag, A., and Sirovich, L. (2000). The approach of a neuron population firing rate to a new equilibrium: an exact theoretical result. *Neural Computation*, 12(5):1045–1055.

Knösche, T. R. (2014). Jansen-Rit Model. In *Encyclopedia of Computational Neuroscience*, pages 1–5. Springer New York, New York, NY.

Kuramoto, Y. (1984). *Chemical Oscillations, Waves, and Turbulence*, volume 19 of *Springer Series in Synergetics*. Springer Berlin Heidelberg, Berlin, Heidelberg.

Laing, C. R. (2009). The dynamics of chimera states in heterogeneous Kuramoto networks. *Physica D: Nonlinear Phenomena*, 238(16):1569–1588.

Laing, C. R. (2014). Derivation of a neural field model from a network of theta neurons. *Physical Review E*, 90(1):010901.

Laing, C. R. (2015). Exact Neural Fields Incorporating Gap Junctions. *SIAM Journal on Applied Dynamical Systems*, 14(4):1899–1929.

Laing, C. R. (2016a). Bumps in Small-World Networks. *Front Comput Neurosci*, 10(June):53.

Laing, C. R. (2016b). Travelling waves in arrays of delay-coupled phase oscillators. *Chaos*, 26(9).

Latham, P. E., Richmond, B. J., Nelson, P. G., and Nirenberg, S. (2000). Intrinsic dynamics in neuronal networks. I. Theory. *Journal of Neurophysiology*, 83(2):808–827.

Liley, D. T. J. (2013). Neural Population Model. In *Encyclopedia of Computational Neuroscience*, pages 1–17. Springer New York, New York, NY.

Lopes da Silva, F. H., Hoeks, A., Smits, H., and Zetterberg, L. H. (1974). Model of brain rhythmic activity - The alpha-rhythm of the thalamus. *Kybernetik*, 15(1):27–37.

Luke, T. B., Barreto, E., and So, P. (2013). Complete classification of the macroscopic behavior of a heterogeneous network of theta neurons. *Neural Comput.*, 25(12):3207–3234.

Lund, J. S., Angelucci, A., and Bressloff, P. C. (2003). Anatomical substrates for functional columns in macaque monkey primary visual cortex. *Cerebral Cortex*, 13(1):15–24.

McCulloch, W. S. and Pitts, W. (1943). A logical calculus of the ideas immanent in nervous activity. *The Bulletin of Mathematical Biophysics*, 5(4):115–133.

Montbrió, E., Pazó, D., and Roxin, A. (2015). Macroscopic description for networks of spiking neurons. *Physical Review X*, 5(2):1–15.

Mountcastle, V. B. (1957). Modality and Topographic Properties of Single Neurons of Cat's Somatic Sensory Cortex. *Journal of Neurophysiology*, 20(4):408–434.

Naud, R. and Gerstner, W. (2012). Coding and Decoding with Adapting Neurons: A Population Approach to the Peri-Stimulus Time Histogram. *PLoS Computational Biology*, 8(10).

Nunez, P. L. (1974). The brain wave equation: a model for the EEG. *Mathematical Biosciences*, 21(3-4):279–297.

Nykamp, D. and Tranchina, D. (2000). A population density approach that facilitates large-scale modeling of neural networks: analysis and an application to orientation tuning. *Journal of computational neuroscience*, 8(1):19–50.

O'Keeffe, K. P. and Strogatz, S. H. (2016). Dynamics of a population of oscillatory and excitable elements. *Physical Review E*, 93(6):1–8.

Omel'chenko, O. E. (2013). Coherence–incoherence patterns in a ring of non-locally coupled phase oscillators. *Nonlinearity*, 26(9):2469.

Omel'chenko, O. E., Wolfrum, M., and Laing, C. R. (2014). Partially coherent twisted states in arrays of coupled phase oscillators. *Chaos: An Interdisciplinary Journal of Nonlinear Science*, 24(2):023102.

Omurtag, A., Knight, B. W., and Sirovich, L. (2000). On the simulation of large populations of neurons. *J Comput Neurosci*, 8:51–63.

Ott, E. and Antonsen, T. M. (2008). Low dimensional behavior of large systems of globally coupled oscillators. *Chaos (Woodbury, N.Y.)*, 18(3):037113.

Ott, E. and Antonsen, T. M. (2009). Long time evolution of phase oscillator systems. *Chaos*, 19(2).

Ott, E., Hunt, B. R., and Antonsen, T. M. (2011). Comment on "Long time evolution of phase oscillators systems". *Chaos*, 21:25112.

Pazó, D. and Montbrió, E. (2014). Low-dimensional dynamics of populations of pulse-coupled oscillators. *Phys. Rev. X*, 4:011009.

Pazó, D. and Montbrió, E. (2016). From Quasiperiodic Partial Synchronization to Collective Chaos in Populations of Inhibitory Neurons with Delay. *Physical Review Letters*, 116(23):238101.

Pinto, D. J. and Ermentrout, G. B. (2001). Spatially Structured Activity in Synaptically Coupled Neuronal Networks: I. Traveling Fronts and Pulses. *SIAM Journal on Applied Mathematics*, 62(1):206–225.

Rankin, J., Avitabile, D., Baladron, J., Faye, G., and Lloyd, D. J. B. (2014). Continuation of Localized Coherent Structures in Nonlocal Neural Field Equations. *SIAM Journal on Scientific Computing*, 36(1):B70–B93.

Ratas, I. and Pyragas, K. (2016). Macroscopic self-oscillations and aging transition in a network of synaptically coupled quadratic integrate-and-fire neurons. *Physical Review E - Statistical, Nonlinear, and Soft Matter Physics*, 94(3):1–11.

Richardson, M. J. E. (2007). Firing-rate response of linear and nonlinear integrate-and-fire neurons to modulated current-based and conductance-based synaptic drive. *Physical Review E - Statistical, Nonlinear, and Soft Matter Physics*, 76(2):1–15.

Richardson, M. J. E. (2009). Dynamics of populations and networks of neurons with voltage-activated and calcium-activated currents. *Physical Review E - Statistical, Nonlinear, and Soft Matter Physics*, 80(2):1–16.

Risken, H. (1989). *The Fokker-Planck equation : methods of solution and applications*. Springer-Verlag, Berlin New York.

Roxin, A., Brunel, N., and Hansel, D. (2005). Role of delays in shaping spatiotemporal dynamics of neuronal activity in large networks. *Physical review letters*, 94(23):238103.

Roxin, A. and Montbrió, E. (2011). How effective delays shape oscillatory dynamics in neuronal networks. *Physica D: Nonlinear Phenomena*, 240(3):323–345.

Schaffer, E. S., Ostojic, S., and Abbott, L. F. (2013). A Complex-Valued Firing-Rate Model That Approximates the Dynamics of Spiking Networks. *PLoS Computational Biology*, 9(10):e1003301.

Silberberg, G., Bethge, M., Markram, H., Pawelzik, K., and Tsodyks, M. (2004). Dynamics of Population Rate Codes in Ensembles of Neocortical Neurons. *Journal of Neurophysiology*, 91(2):704–709.

So, P., Luke, T. B., and Barreto, E. (2014). Networks of theta neurons with time-varying excitability: Macroscopic chaos, multistability, and final-state uncertainty. *Physica D*, 267(0):16–26.

Stein, R. B. (1965). A Theoretical Analysis of Neuronal Variability. *Biophysical Journal*, 5(2):173–194.

Stein, R. B. (1967). Some Models of Neuronal Variability. *Biophysical Journal*, 7(1):37–68.

Tchumatchenko, T., Malyshev, A., Wolf, F., and Volgushev, M. (2011). Ultrafast Population Encoding by Cortical Neurons. *Journal of Neuroscience*, 31(34):12171–12179.

Tiesinga, P. H. E. and Jose, J. V. (2000). Robust gamma oscillations in networks of inhibitory hippocampal interneurons. *Network-Computation In Neural Systems*, 11(1):1–23.

Touboul, J. (2012). Mean-field equations for stochastic firing-rate neural fields with delays: Derivation and noise-induced transitions. *Physica D: Nonlinear Phenomena*, 241(15):1223–1244.

Tuckwell, H. C. (1988). *Introduction to theoretical neurobiology - volume 1*. Cambridge university press.

Veltz, R. (2013). Interplay between synaptic delays and propagation delays in neural field equations. *SIAM Journal on Applied Dynamical Systems*, 12(3):1566–1612.

Wang, X.-J. (2010). Neurophysiological and computational principles of cortical rhythms in cognition. *Physiological reviews*, pages 1195–1268.

Wang, X.-J. and Buzsáki, G. (1996). Gamma Oscillation by Synaptic Inhibition in a Hippocampal Interneuronal Network Model. *The Journal of Neuroscience*, 16(20):6402–6413.

Weiss, T. F. (1966). A model of the peripheral auditory system. *Kybernetik*, 3(4):153–175.

White, J. A., Chow, C. C., Ritt, J., Soto-Treviño, C., and Kopell, N. (1998). Synchronization and oscillatory dynamics in heterogeneous, mutually inhibitory networks. *J. Comput. Neurosci.*, 5:5–16.

Whittington, M. A., Cunningham, M. O., LeBeau, F. E., Racca, C., and Traub, R. D. (2011). Multiple origins of the cortical gamma rhythm. *Developmental Neurobiology*, 71(1):92–106.

Whittington, M. A., Traub, R. D., and Jefferys, J. G. R. (1995). Synchronized oscillations in interneuron networks driven by metabotropic glutamate receptor activation.

Whittington, M. A., Traub, R. D., Kopell, N., Ermentrout, B., and Buhl, E. H. (2000). Inhibition-based rhythms: Experimental and mathematical observations on network dynamics. *International Journal of Psychophysiology*, 38(3):315–336.

Wilson, H. R. and Cowan, J. D. (1972). Excitatory and inhibitory interactions in localized populations of model neurons. *Biophysical journal*, 12(1):1–24.

Wilson, H. R. and Cowan, J. D. (1973). A mathematical theory of the functional dynamics of cortical and thalamic nervous tissue. *Kybernetik*, 13(2):55–80.

Zhang, L. (2007). How Do Synaptic Coupling and Spatial Temporal Delay Influence Traveling Waves in Nonlinear Nonlocal Neuronal Networks? *SIAM Journal on Applied Dynamical Systems*, 6(3):597–644.